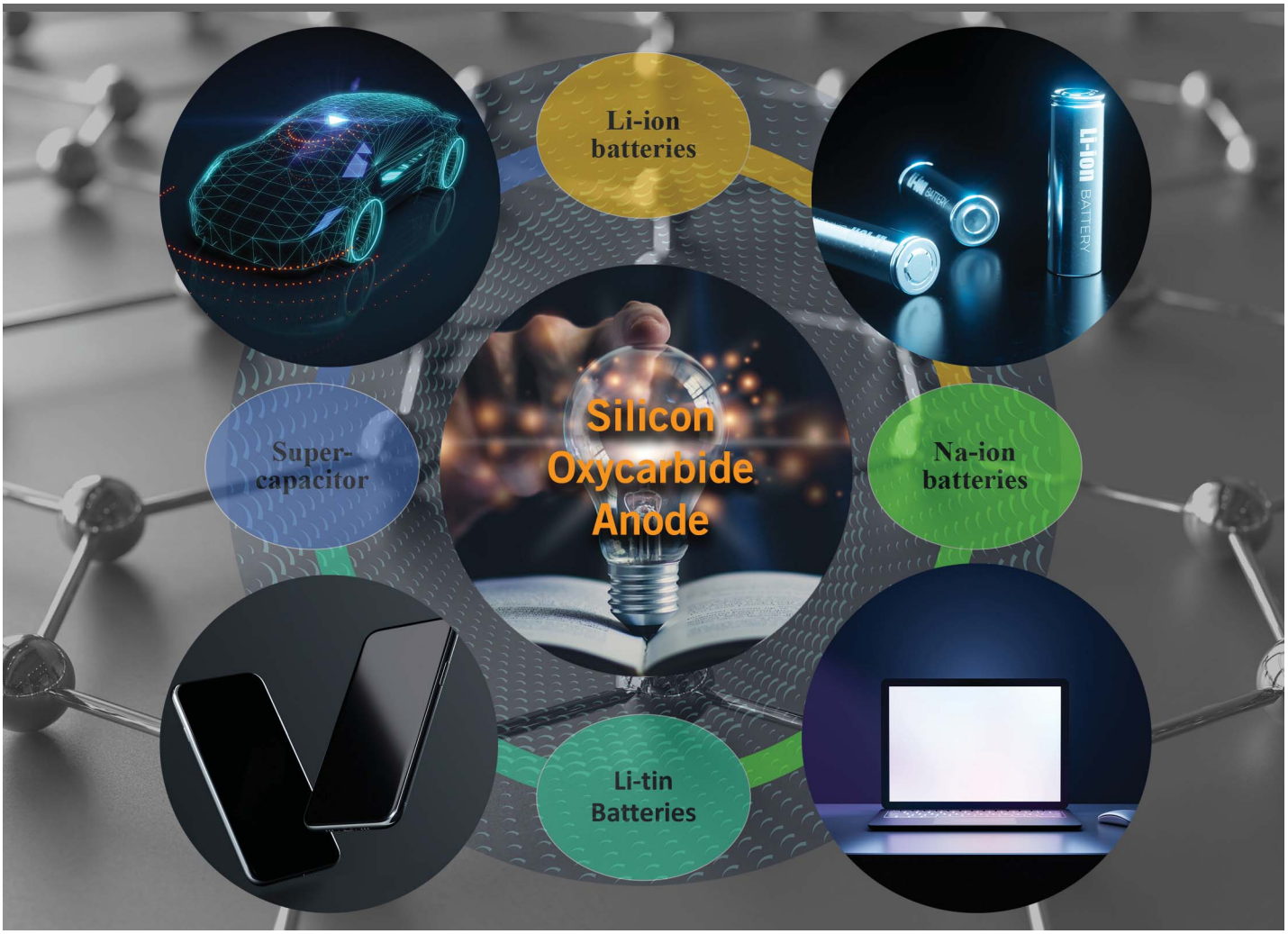

Silicon oxycarbide as an anode material for lithium-ion batteries and beyond: Research from Prof. Sujith & Dr. Jella at BITS Pilani, Hyderabad, and Prof. Rajendra Bordia and Dr. Dillip K. Panda at Clemson University's Department of Materials Science and Engineering.

A review of silicon oxycarbide ceramics as next generation anode materials for lithium-ion batteries and other electrochemical applications

The silicon oxycarbide ceramics synthesized *via* a precursor-derived ceramic route are promising anode materials for lithium-ion batteries with specific capacities between 200-1300 mAh/g. Contrary to crystalline silicon, these amorphous materials can accommodate significant volumetric strains. This article discusses the various factors that influence SiOC's electrochemical performance and techniques for overcoming them.

As featured in:

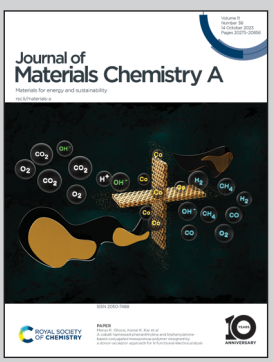

See Dillip K. Panda *et al.*, *J. Mater. Chem. A*, 2023, **11**, 20324.

ROYAL SOCIETY OF CHEMISTRY

rsc.li/materials-a

Registered charity number: 207890

Journal of Materials Chemistry A

REVIEW

View Article Online
View Journal | View Issue

Cite this: J. Mater. Chem. A, 2023, 11, 20324

A review of silicon oxycarbide ceramics as next generation anode materials for lithium-ion batteries and other electrochemical applications

Ravindran Sujith, [ab] Jella Gangadhar,[a] Michelle Greenough,[c] Rajendra K. Bordia[c] and Dillip K. Panda*[c]

Received 6th March 2023
Accepted 30th June 2023

DOI: 10.1039/d3ta01366a

rsc.li/materials-a

Lithium-ion batteries (LIBs) are the energy storage system of choice for the electrification of transportation and portable electronics. They are also being actively considered to meet the need to store electricity produced by renewable sources which tend to produce electricity intermittently. In commercial LIBs, graphite is the most common anode material. However, its theoretical specific capacity (372 mA h g^{-1}) is limited. A search for alternatives led to the development of Si anodes due to their extremely high theoretical specific capacities (4200 mA h g^{-1}). However, their commercial viability is limited due to their high volumetric expansion (more than 300%), which results in capacity fading during cycling. Silicon oxycarbide (SiOC) materials, which are synthesized using a polymer-derived ceramic (PDC) route, have been investigated as a substitute anode material for crystalline Si-based anodes. The specific capacity of these SiOC materials ranges from 200–1300 mA h g^{-1}. Furthermore, these SiOCs are tailorable to meet the needs of electrochemical applications due to their versatile synthesis routes. Moreover, the amorphous nature of these materials and their micro–mesoporous structure make them capable of accommodating large strains when charged or discharged. In this review, we discuss the various factors that influence SiOCs' electrochemical performance, storage mechanisms, and recent developments.

[a]Mechanical Engineering Department, Birla Institute of Technology and Science Pilani, Hyderabad Campus, 500078, India
[b]Materials Center for Sustainable Energy and Environment, Birla Institute of Technology and Science Pilani, Hyderabad Campus, 500078, India
[c]Department of Materials Science and Engineering, Clemson University, Clemson, SC, 29634, USA. E-mail: dpanda@g.clemson.edu

Sujith is currently working as an associate professor in the Mechanical Engineering Department at BITS Pilani, Hyderabad Campus. He received his B. Tech from Kerala University, M. Tech from NIT Calicut (gold medallist) and PhD degree from Indian Institute of Technology, Madras. He received the Early Career Research Award in 2016 from the Department of Science and Technology, Govt. of India, for pursuing research in the development of hydrogen storage materials. His research is mainly focused towards developing materials for energy storage applications, mechanical deformation behaviour of metals and composites, theoretical studies involving DFT, etc. He has contributed to more than 45 international journal publications and 2 book chapters.

Gangadhar obtained his B. Tech and M. Tech degrees from NCET and GRIET, affiliated to Jawaharlal Nehru Technological University, Hyderabad (JNTUH). He obtained his PhD degree from Birla Institute of Technology and Sciences - Pilani, Hyderabad campus, under the supervision of Prof. Ravindran Sujith and co-supervision of Prof. Rajendra K. Bordia of Clemson University. His research interests include development of high energy density anode materials for Li-ion batteries and a specific focus on the materials which include polymer derived silicon oxycarbide, silicon, and silicon derived from rice husk and graphene-based composites. He has authored around 7 peer-reviewed journal publications and a book chapter and participated in 10 international conferences.

SiOC anodes suffer from low electrical conductivity, low Coulombic efficiencies, large hysteresis, and high first-cycle losses. Several techniques, such as employing nanoparticles, prelithiation, and using thin-film geometries, have been employed to overcome these limitations. The literature on these approaches is also reviewed. A number of recent studies have also examined the use of SiOC in lithium-tin anodes, sodium-ion batteries, and supercapacitors. The status of these developments and the challenges associated with the wide-scale use of SiOC is presented.

1. Introduction

We are on the path to transitioning from internal combustion engine-based mobility to electric vehicles, and lithium-ion batteries (LIBs) play an important role in achieving this target.[1] Compared to conventional lead-acid and nickel-cation batteries, LIBs have gained considerable interest owing to their high energy and power densities, better safety, and long cycling stability.[2] As an anode material, graphite is most commonly used in LIBs. It has a theoretical capacity of 372 mA h g^{-1} in a lithiated state (LiC_6).[3] The capacity mentioned above, however, is not sufficient to meet the ever-increasing global demand for higher energy densities, requiring the development of alternative materials capable of providing higher energy densities. Due to its high theoretical capacity of 4200 mA h g^{-1} and low working voltage of 0.4 V,[4] Si has garnered much attention among the possible alternatives. Although Si-based anodes are attractive, their applications are limited due to their high volumetric expansion (300%) and poor electrical conductivity. High volumetric strain leads to pulverization of Si-

Michelle Greenough has a B.S. in chemistry with minors in biology and mathematics from Wagner College, NY. In 2015, she joined Prof. Bordia's group at Clemson University, to pursue her PhD She was a recipient of the National Science Foundation (NSF) Graduate Research Fellowship in 2016. She also received the NSF INTERN Fellowship which she used to conduct research in France and Germany. And she was a recipient of the Materials Science Department's Gilbert Robinson Memorial Fellowship. She completed her PhD in August 2021 and is currently a staff scientist at the Lawrence Livermore National Laboratories.

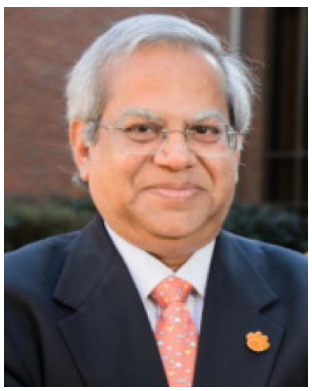

Bordia is currently the George J. Bishop, III Professor of Ceramic and Materials Engineering in the Department of Materials Science and Engineering at Clemson University in Clemson, SC, USA. He was a faculty member at the University of Washington (1991–2013) and a research scientist at DuPont Co. (1986 to 1991). He received his B. Tech from IIT, Kanpur, India (1979), and his M.S. (1981) and PhD (1986) from Cornell University, Ithaca, NY, USA. His research is at the intersection of materials and mechanics and is focused on fundamental and applied studies in the processing and properties of complex material systems for energy, environmental and medical applications. He has authored or co-authored over 170 peer-reviewed technical publications.

Dr Panda is currently working as a research assistant professor in the Department of Materials Science and Engineering at Clemson University. Prior to joining Clemson University, Dillip worked at Florida State University (Tallahassee) and University of Michigan (Ann Arbor) as a postdoctoral fellow. He has received his M.Sc. (gold medal) in chemistry from NIT-Rourkela, India. He completed his PhD from the University of Wollongong (Australia) in 2011 under the tutelage of Prof. Gordon G Wallace. Throughout his career this work has led to more than 30 peer-reviewed publications in various journals (e.g., JACS, Chem. Commun., Chem. Sci., ACS Appl. Mater. Interfaces, ACS Sustainable Chem. Eng., J. Mater. Chem. C, Langmuir, Inorganic Chemistry, Organic Letters, etc.) and three separate book chapters. His current research focuses on approaches to high-temperature all solid-state lithium batteries for electric vehicles and Li-ion batteries. His research has been presented in different parts of the world, including India, Australia, Italy, and the United States. Also, Dr Panda was the president of the Clemson University Postdoctoral Association from 2020 to 2022 and the recipient of the Clemson University Distinguished Postdoctoral Award for 2022, among other honors.

Table 1 The properties of various materials employed as anodes in LIBs

S. no	Anode materials	Theoretical capacity (mA h g^{-1})	Electrochemical potential (V)	Volume expansion (%)	Electrical conductivity (S m^{-1})	Density (g/cc)
1	Graphite[14,15]	372	0.1	13.2	1.2×10^{5}	2.25
2	Silicon[14,15]	4200	0.4	323	6.7×10^{-2}	2.30
3	Lithium[14,15]	3860	3.04	—	1.1×10^{7}	0.53
4	Lithium titanium oxide[14,15]	330	1.5	1	7.5×10^{-5}	3.43
5	Tin[14,15]	994	0.6	260	9.1×10^{6}	7.31
6	Antimony[14,15]	660	0.9	200	2.5×10^{6}	6.68
7	Silicon oxycarbide	1300 (maximum)[16]	<0.5 (ref. 17)	22 (ref. 18)	3×10^{-8}–2.2 (ref. 19)	1.80–2.30 (ref. 20)

anodes leading to capacity fading in these cells.[5] Many efforts have been made, and are continuing to be made, to overcome this constraint, including nanostructuring and embedding Si particles in another matrix.[6–12] Although these efforts have been made, commercialising the Si anodes remains a substantial challenge, in part, because of their high fabrication costs, complexities in processing, and low volume production.[13] The properties of various materials employed as anodes in LIBs are presented in Table 1.

Compared to crystalline Si, silicon oxycarbides (SiOCs) offer high structural stability, low volumetric expansion (22%), ease of fabrication, and large-scale production capability.[21,22] One of the most efficient methods for the synthesis of SiOC ceramics is the polymer-derived ceramic (PDC) route, wherein a suitable polymeric precursor is pyrolyzed in a controlled atmosphere to produce the required ceramic. It is possible to achieve better control over the composition of the ceramic *via* the PDC route compared to other processing routes such as sol–gel processing. The pyrolysed ceramics are typically amorphous in nature consisting of $SiO_{4-x}C_x$ tetrahedral units. The amorphous nature of the ceramics is crucial for battery applications as it can accommodate volumetric strains during Li-ion insertion. In addition, depending on the polymeric precursor chemistry, a little or considerable amount of disordered carbon (free carbon) is produced during the pyrolysis process, which could act as efficient charge carriers and active sites for Li-ion insertion. Moreover, the presence of micro–mesoporosities provides an additional buffer for these PDCs to accommodate volumetric strains.[23–25]

In the literature, SiOC anodes' capacities have been reported to be between 200 and 1300 mA h g^{-1}, likely due to structural differences in the SiOC ceramic used to fabricate these anodes. During the production of PDCs, precursor chemistry and processing parameters have a strong influence on the final phase composition and microstructure of the ceramic. A number of other factors have also been reported to influence the energy storage mechanisms of SiOCs, including the amount of free carbon, the fraction of tetrahedral units, and the porosity.[26–29]

Although the specific capacity that can be achieved is double that of the commercially existing graphite and there is the advantage of ease of processing, SiOC also faces other challenges as an anode material, including high first cycle irreversibility, voltage hysteresis, low electrical conductivity and lower capacity than that of pristine silicon. The main challenge is its low Coulombic efficiency (40–70%), especially during the first cycle, due to the irreversible nature of alloying reactions between Li and Si.[4] There is also a limitation of its low electrical conductivity, with values ranging from 10^{-5} S m^{-1} to 2 S m^{-1} depending on the amount of free carbon in the material and its structure.[30] Although free carbon can lead to better conductivity than pure Si, SiOCs have displayed lower conductivities for LIB applications because of the open structure of free carbon and the lack of the sufficient volume fraction of carbon necessary to form the desired percolating network.[31] Nevertheless, these limitations can be overcome by controlling the initial precursor chemistry and developing composite anodes.[29,30,32,33] Additionally, strategies such as pre-lithiation, synthesis of spherical and thin-film anodes, *etc.*, can enhance the reversible storage capacity and Coulombic efficiency of these systems.[34,35]

In the literature, readers can find several detailed review papers on polymer-derived ceramics which include their synthesis and characterisation.[20,36–48] To our knowledge, there have been no reviews that focus exclusively on suitability of SiOCs as anodes in LIBs and other electrochemical applications. The purpose of this review is therefore to discuss factors influencing the electrochemical properties of SiOCs, existing challenges, and strategies for overcoming them.

2. Synthesis of polymer-derived silicon oxycarbide ceramics

PDCs are synthesized by pyrolyzing polymeric precursors in a controlled atmosphere. Verbeek *et al.* were the first to demonstrate polymer to ceramic transformation by the pyrolysis route. They synthesized SiC by pyrolysis of polysilanes in a controlled atmosphere.[49] In later studies, Fritz and Raabe, and Yajima and co-workers made significant breakthroughs in PDC synthesis.[50,51] A variety of silicon-based polymer precursors have been researched over the past 50 years, and Fig. 1 shows the families of the important polymeric precursors that have been used in the field of PDCs. Since SiOC ceramics are easy to synthesize and readily available, they have been gaining much attention.[39] Aside from that, these PDCs have shown excellent chemical and thermal stability, making them suitable for a variety of functional applications, including energy storage, high-temperature sensors, microelectromechanical systems, drug delivery, filters and catalysis.[21,38,46,47]

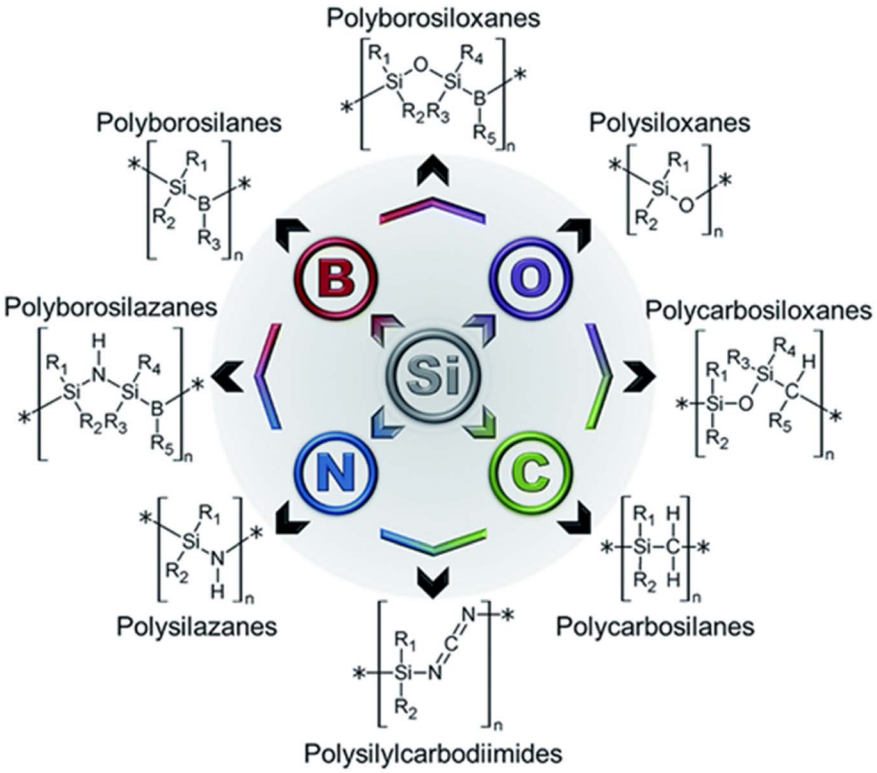

Fig. 1 Overview of the various polymeric precursors used in the synthesis of PDCs.[39] Reproduced with permission from ref. 39. Copyright 2019, Royal Society of Chemistry.

The ceramic obtained by the pyrolysis of a polysiloxane could result in an open network-like structure consisting of amorphous phases of SiOC with $SiO_{4-x}C_{x\ (x=1-4)}$ structural units and disordered carbon (free carbon).[20] The final structure of the ceramic is controlled by the choice of the polymeric precursors and the processing parameters (*e.g.* method of crosslinking,

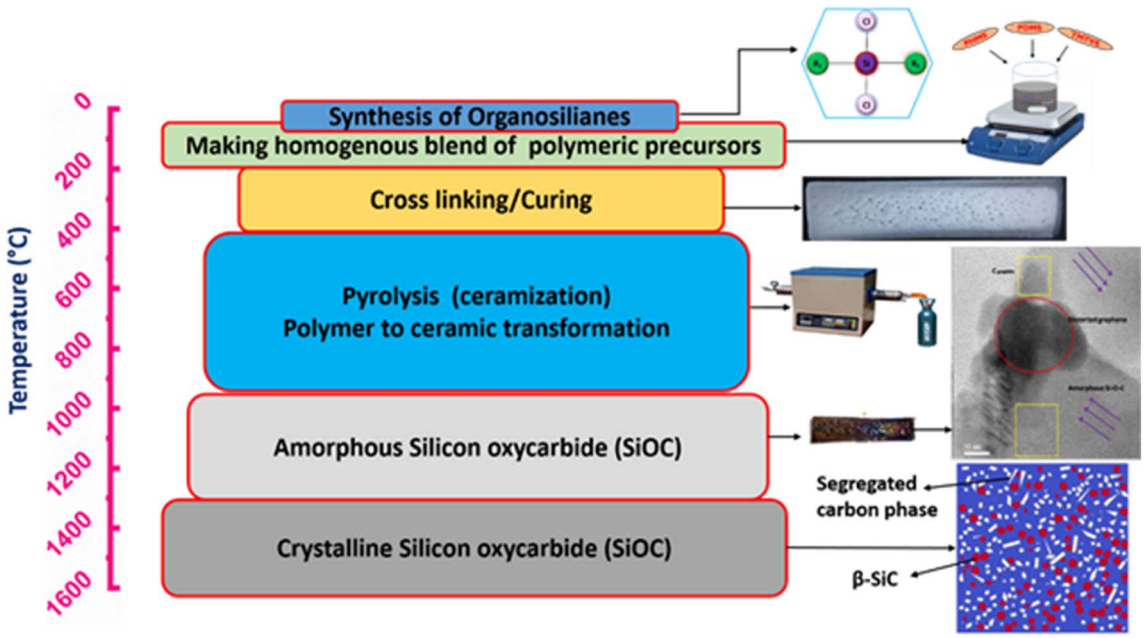

Fig. 2 Schematic illustration of the synthesis procedure of the polymer-derived silicon oxycarbide ceramic.[38,39,55] The idea for designing the schematic was taken from ref. 38 and 39. The TEM image is reproduced with permission from ref. 55 Copyright 2018, Springer Nature. The SiC segregated carbon phase image is reproduced with permission from ref. 53, Copyright 2018, MDPI.

pyrolysis temperature and atmosphere). The schematic representation of the synthesis procedure of a polymer-derived SiOC ceramic is shown in Fig. 2. It is possible to customize the final ceramic material using the parameters provided in the schematic (Fig. 2). In addition, with increasing pyrolysis temperatures (>1200 °C), carbothermic reduction could take place resulting in phase separation and crystallization of SiOC,[52–54] which may be unsuitable for battery applications.

In general, the precursors used to synthesize SiOC PDCs can be classified into Si-rich and C-rich precursors to better comprehend the mechanisms of their energy storage. For achieving C-rich SiOC, various strategies have been employed, including the use of precursors that have phenyl groups,[28,56,57] and the addition of divinylbenzene (DVB).[58,59] In spite of this, there may be a threshold limit beyond which free carbon becomes destabilised.[59] Therefore, it is imperative to control the size of free carbon domains. A study found that DVB facilitates the formation of free carbon and silicon oxycarbide bonds.[58] Furthermore, the presence of free carbon could be beneficial to the fabrication of LIBs as it improves their electrical conductivity.[30] A silicon-rich SiOC can be synthesized through the pyrolysis of polymeric precursors such as tetraethoxysilane, polyhydroxymethylsiloxane, cyclic 2,4,6,8-tetramethyl-2,4,6,8 tetravinlycyclotetrasiloxane,1,3,5,7-tetramethyl-1,3,5,7-tetravinylcyclotetrasiloxane (TTCS) and silicone oil. SiOC systems would be predominantly silicon-rich if silicon-based polymeric precursors did not contain phenyl or alkyl groups in the precursor. However, it should be noted that the Si-rich SiOCs contain free carbon, albeit in low concentrations.[58]

The porosity of PDCs also plays a key role in determining their usefulness as anodes for LIBs. As a result of the escape of various volatile materials during pyrolysis, PDCs are inherently porous. By tuning the process parameters and modifying precursor chemistry, it is possible to achieve the desired porosity levels.[43] Porosity can be further tuned to the desired level by employing various strategies such as hydrofluoric acid etching, infiltration, and the use of sacrificial template techniques.[17,24,60–64] It has been observed that the porosity improves the cycling stability of LIBs by accommodating the volume expansion. However, a high level of porosity compromises transport of Li ions and mechanical properties. Thus, there is a requirement for synthesising SiOCs with an optimum level of porosity.[23,29]

3. Mechanisms of electrochemical storage

The Li-ion storage in SiOC typically exhibits a dual mechanism involving intercalation and alloying processes (Fig. 3a and b). The presence of silica tetrahedral units facilitates alloying, whereas the free carbon facilitates intercalation. Depending on whether the material is silicon rich or carbon rich, the dominant mechanism can be illustrated. Liu *et al.* studied the Li-ion storage mechanism of SiOC by performing various characterization techniques such as ^{29}Si magic angle spinning nuclear magnetic resonance (NMR), Si X-ray photoelectron spectroscopy and cyclic voltammetry.[65] In their study they have postulated that there exist four species/resonances in the SiOC sample such as SiO_4, SiO_3C, SiO_2C_2 and $SiOC_3$, out of which SiO_3C and SiO_2C_2 are electrochemically active to Li ions and contribute towards reversible capacity whereas $SiOC_3$ is irreversibly converted into SiC_4 after the first cycle. The active SiO_4 phase resulted in Li_2SiO_3 on intercalation, whereas the inactive part resulted in Li_4SiO_4. Studies by Xue *et al.* showed that irreversible capacity, associated with the initial cycle charge/discharge of a SiOC increases with the increase of silicon and oxygen contents.[66] Contrary to Liu *et al.*, other studies have showed that the carbon phase is the major Li-ion storage host site.[65] It has been shown that lithium is accommodated in interstitial and defect sites and edges of graphene sheets, and adsorbed on the interface of graphite nano-crystallites in carbon-rich SiOC.[24,27,67–69] Furthermore, ^{7}Li MAS NMR measurements performed by Fukui *et al.* confirm the presence of at least two electrochemically active sites for lithium storage in the SiOC

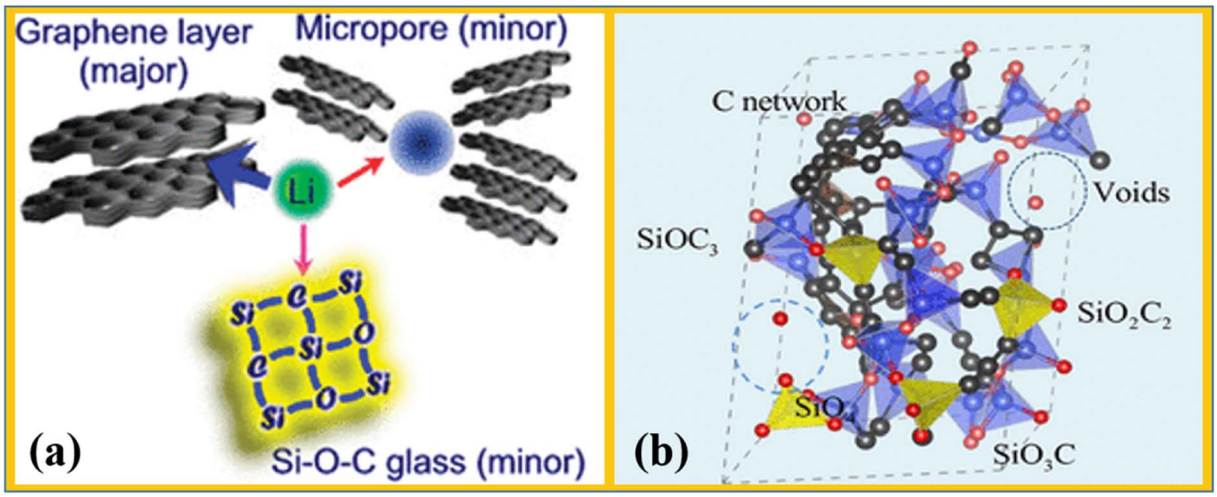

Fig. 3 Mechanism of Li-ion storage in SiOC for (a) carbon rich[67] and (b) silicon rich material systems.[18] Reproduced with permission from ref. 67. Copyright 2010, Reproduced with permission from ref. 18. Copyright 2017. American Chemical Society.

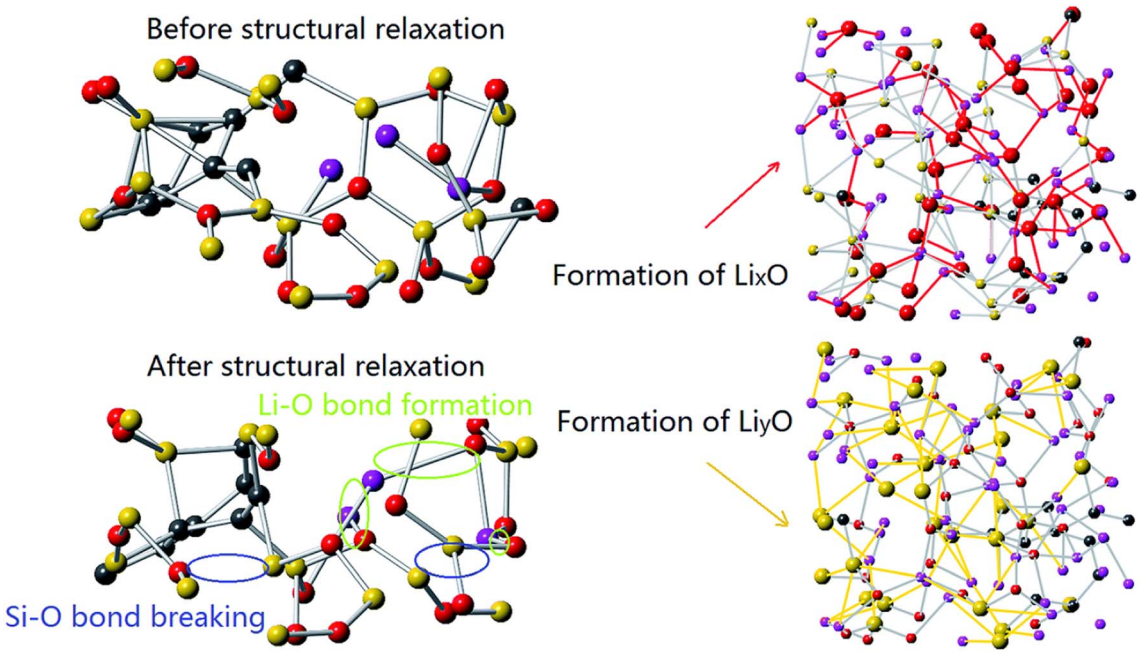

Fig. 4 The zoomed-in structures of lithiated $SiC_{2/5}O_{6/5}$. Thepicture on the left shows Li incorporation through the breaking of Si–O bonds and the formation of Li–O bonds, and the image on the right describes the formation of Li_xO and Li_ySi complexes.[71] Reproduced with permission from ref. 71. Copyright 2016, Royal Society of Chemistry.

composite materials, out of which the carbon phase is the major host site for lithium storage.[70] Additionally, extensive structural and electrochemical studies reveal that the micropores present in SiOC can act as active sites for lithium storage resulting in better reversibility in the range of 0.005–0.4 V.

4. First principles studies

Studies based on first principles revealed that the atomic structure and bonding mechanism play an important role in the lithiation process.[18,71–75] The insertion of Li-ions in SiOC ceramics with different carbon contents was investigated by Liao and co-workers using density functional theory (DFT) calculations.[71] Fig. 4 illustrates the lithiated state of the various structures. It is concluded from their study that the Li atom prefers to bond with oxygen atoms and stays near carbon atoms in the empty spaces. Therefore, based on their research, it can be concluded that a high carbon content results in better reversible storage capacities, which is supported by experimental observations.[71] In addition, DFT studies have shown that carbon in the segregated form stabilises the whole system by forming 3D networks. They have also calculated the formation energy of the lithiated systems and reported that the most stable compositions for $Li_xSiC_{2/5}O_{6/5}$, $Li_xSiCO_{6/5}$, and $Li_xSiC_{8/5}O_{6/5}$ are $x = 2.75$, 3.25 and 4. These correspond to theoretical specific capacities of 1415, 1470 and 1613 mA h g^{-1}, respectively.[75] SiOC has also been found to have a favorable lithium insertion process compared to SiO_2, possibly because it has a larger free volume than SiO_2.[73] A similar study by Sun and Zhao *et al.* on the atomistic origin of the performance of carbon-rich SiOC, demonstrates a two-step process of lithium insertion: (i) Li ions adsorb onto nano-voids followed by (ii) accommodation of the Li ions in the SiOC, segregated carbon network and the defect sites. They have also observed that a maximum volumetric expansion of 22% can occur in these systems at a fully lithiated capacity of 1230 mA h g^{-1}.[18] Kroll *et al.* also found that the storage of lithium ions in amorphous silica and SiOC without segregated carbon is energetically unfavourable because of a large bandgap, whereas the bandgap of SiOC ceramics can be reduced considerably by the presence of the low-laying unoccupied states arising from the free carbon phase.[76] Furthermore, it is also ascertained that the free carbon facilitates lithium ion bonding to oxygen sites *via* improving the electronic conduction, leading to irreversible lithium uptake. On the other hand, the free carbon also contributes to a major part of the reversible lithium storage capacity.

Furthermore, first principles studies on five different SiOC structures have shown that Li_2O tends to form initially due to the cleavage of Si–O, and later Li_xO and Li_ySi form with increasing lithium-ion concentration.[71] Interestingly, carbon does not attract lithium ions in such systems but stabilizes them by forming stable C–C bonds. They have also reported that the free volume decreases with the carbon content; hence, the voids have an insignificant role in the better electrochemical performance. Furthermore, as observed experimentally, the reversible capacity increases with increasing carbon weight fraction, but beyond a threshold value, it tends to decrease with an increase in carbon content.[71] However, another study revealed that, at least initially, the Li ions occupy the microvoids present in SiOC. Subsequent insertion could lead to the cleavage of Si–O and Si–C, leading to larger free volumes.[72] They have also estimated the theoretical storage capacities in O-rich

$SiO_{1.5}C_{0.5}$ and C-rich $SiO_{0.5}$ $C_{1.5}$, and the corresponding values for Li^+ are 519 and 681 mA h g^{-1}; Na^+ are 335 and 186 mA h g^{-1}; K^+ are 335 and 681 mA h g^{-1}, respectively. The repulsion-created structural instability is the reason for K^+ions' relatively low storage capacities, whereas favourable Li–Si formation is responsible for the higher storage capacity of Li^+ ions.[72] However, it has been reported that local compressive stresses are generated in the lithiated systems resulting in the shortening of bond lengths and a higher bulk modulus.[77] This also means that the local stress generated can be used to measure the system's specific capacity. Moreover, it is observed that replacing oxygen with nitrogen in these systems makes it unattractive for lithium intercalation due to the highly covalent nature of Si–N bonds and the lower electron density of nitrogen atoms.[78] Hence, silicon carbonitrides are expected to exhibit lower storage capacities in comparison to silicon nitrides, and experimental evidence also supports this.[79–81]

5. Factors affecting the electrochemical properties of SiOC anodes

5.1 Presence of free carbon

Anodes fabricated from amorphous SiOC ceramics prepared by the thermolysis of phenyl-substituted branched polysilane ($(Ph_2Si)0.85(PhSi)0.15$) and polystyrene (1 : 1 by weight) have shown a capacity of more than 600 mA h g^{-1}. In these systems, the Li ions are electrochemically stored in the interstitial spaces of the free carbon in the SiOC phase and the micropores. The system chosen was C-rich, and thus, the interlayer spacing within the free carbon contributed more to electrochemical storage, suggesting that an increase in free carbon content might be able to increase the storage capacity of the battery.[17] Furthermore, other studies have also shown that free carbon in the disordered form offers higher Li-ion storage sites in comparison to ordered free carbon.[56,58] Wilamowska and co-workers synthesised SiOC ceramics with varying carbon contents (from 25 to 40 wt%) and demonstrated that the reversible capacity improves with the carbon content. However, there seems to be no linear relation between the free carbon content and electrochemical performance.[56] Contrary to previous observation, Monika and co-workers demonstrated a linear relation between the carbon content and electrochemical performance. Carbon-rich samples exhibited much higher capacities (550 mA h g^{-1} at low C rates after 140 cycles) and lower irreversible capacities (360 mA h g^{-1}) than carbon-lean samples.[26] Thus, free carbon in the disordered form is crucial to improving the electrochemical performance of SiOC.

Free carbon has an additional important effect of increasing the electrical conductivity. It was observed that at a carbon content less than 20 wt%, electrical conductivities were less than 3×10^{-5} S m^{-1}. However, the electrical conductivity of the material was improved to 2.2 S m^{-1} by increasing the free carbon content to 54 wt%.[30] In this regard, Kaspar and coworkers noted that a lower carbon content might lead to a lower electrical conductivity and therefore higher irreversibility. This conclusion was reached after observing that the low electrical conductivity system initially showed an initial storage capacity of 1000 mA h g^{-1}, which rapidly diminished with subsequent cycles. In high electrical conductivity systems, the initial storage capacity was lower, but the observed capacities (500 mA h g^{-1}) remained stable after 60 cycles.[30] So, it can be concluded that the presence of free carbon improves the electrical conductivity and cycling stability of SiOC anodes.

The role of free carbon in the electrochemical properties of SiOCs was later systematically determined by Pradeep and coworkers.[16] In their study, they synthesized amorphous SiOC ceramics with free carbon contents ranging from 8 to 50 wt%, maintaining the same O-to-Si atomic ratio. Unlike studies mentioned earlier, their study revealed that SiOC tetrahedral units have a greater impact on reversible capacity than free carbon. Additionally, they observed a linear relationship between SiOC units and Li insertion capacity, which is consistent with the model proposed by Raj and co-workers.[82] Nevertheless, their studies also indicate that 0.5 wt% of free carbon should be present in the system to achieve the desired levels of electrochemical performance. Therefore, it is important to consider both SiOC units and free carbon content when determining a system's storage capacity.

5.2 Microstructure of PDC

There have been several studies carried out using different types of precursors to understand the effect of compositional differences on the reversible storage capacities of SiOCs.[28] According to Halim and co-workers, SiOC was synthesized from phenyl-rich silicone oils and showed a discharge capacity of 800 mA h g^{-1} at a current density of 200 mA g^{-1}. Its better performance is due to its low dimensional expansion (about 7%) during lithium cycling as well as the enhanced mobility of Li^+ within the matrix (diffusivity of Li^+: 5.1×10^{-6} cm^2 s^{-1}).[28] Furthermore, it was shown that O-rich SiOC maximises reversible storage capacity more than their C-rich counterparts.[83] This could be possible because the SiOC tetrahedral unit dominates the free carbon network.

Another significant aspect that influences the electrochemical performance of SiOC systems is the type of Si–C bonds. Graczyk-Zajac and co-workers synthesised SiOC by pyrolysing polysiloxanes in two different atmospheres –CO_2 (oxidising) and Ar (inert).[84] NMR studies on the PDC synthesised in the oxidising atmosphere revealed the absence of Si–C bonds, whereas the PDC synthesised under inert conditions contained C_2SiO_2, $CSiO_3$ and SiO_4. Moreover, the respective free carbon contents in both the ceramics were 37 wt% and 47 wt%. Interestingly, both these systems showed the same initial storage capacity of 1500 mA h g^{-1} during charging. However, the reversible capacity of the Ar-treated sample (~800 mA h g^{-1}) was found to be much higher compared to that of the sample treated under oxidising conditions (~600 mA h g^{-1}).[84] A high concentration of reversible oxygen-containing species such as SiO_4 and SiO_3C may also contribute to the high reversible storage capacity. This characteristic behavior is probably explained by the high ionic character of the Si–O bonds.[65]

5.3 Pyrolysis temperature

In a similar vein, the significance of pyrolysis temperature on battery performance is unclear. Ahn and Raj demonstrated the necessity of mixed bonds for achieving high levels of Li-ion insertion in PDCs.[85] Their study showed that pyrolysis at 1000 °C achieved the maximum reversible storage capacity of 958 mA h g^{-1}. In contrast, the samples processed at 1400 °C showed only 88 mA h g^{-1} of reversible storage capacity.[65] Other studies have also shown a rapid decline in storage capacity as the pyrolysis temperature increased.[69] For instance, Kaspar and co-workers demonstrated that SiOC pyrolysed at 1100 °C exhibited a stable 521 mA h g^{-1} reversible capacity. On the other hand, the one pyrolyzed at 1300 °C exhibited a storage capacity of only 367 mA h g^{-1}. There have been reports of the formation of several crystalline phases by pyrolysis at temperatures greater than 1200 °C, including SiC, SiO_2 and ordered carbon.[86–89] Since SiO_2 and SiC are inactive species and do not contribute to Li storage, such formation of crystalline phases would reduce the storage capacity.[90] A similar study by Riedel's group supports the finding that lithium's storage capacity decreases with increasing pyrolysis temperatures. These deteriorating properties can be attributed to three main reasons: (i) ordering of free carbon, (ii) lower structural stability of free carbon because of phase separation in SiOC and (iii) crystallisation of electrochemically inactive phases like SiC.[90] Furthermore, NMR studies confirmed that ceramics pyrolyzed at high temperatures (1400 °C) contained electrochemically inactive species like SiC_4.[56] One study, however, reported that the SiOC pyrolysed at 1300 °C exhibited a better reversible storage capacity of 780 mA h g^{-1} as compared to the low-temperature pyrolysed system.[16] In their study, they attributed the superior performance of high-temperature pyrolysed SiOC to its exceptional thermodynamic stability, which makes it less prone to irreversible reactions with Li.[16] It is interesting to note that from the cycling stability standpoint, the samples pyrolysed at 800 °C showed a better Coulombic efficiency of 100% and could last 60 cycles compared to samples pyrolyzed at 1000 °C.[85] It is well known that the residual hydrogen content decreases as the pyrolysis temperature increases. Thus, samples pyrolyzed at 800 °C should contain more residual hydrogen than those pyrolyzed at 1000 °C. The hypothesis is that this excess residual hydrogen stabilizes the material.[85] It has also been observed that thermal crosslinking before pyrolysis improves the reversible storage capability. Using thermal crosslinking at 400 °C to synthesize C-rich SiOC, Kaspar and co-workers studied its electrochemical performance. They observed crosslinked systems performing better than directly pyrolysed samples.[88] A summary of the effect of precursors and pyrolysis temperature on the electrochemical performance of SiOC ceramics is shown in Table 2.

6. Strategies to improve the battery performance

6.1 Enhancing the electrical conductivity

Among the major challenges limiting the use of SiOC anodes in LIBs is their low electrical conductivity. Even though disordered carbon is commonly found in these systems, its discrete distribution in the SiOC matrix and disordered structure result in poor conductivity.[83,101,102] The solution to this problem is to produce composite anodes with SiOC mixed with various carbonaceous nanomaterials such as graphite,[103–106] carbon nanotubes,[32,107,108] carbon nanofibers,[13,109–111] graphene[33,112–120] and reduced graphene oxide.[121,122] Graphene, however, is widely explored among these carbonaceous materials due to its high electrical conductivity.[31,55,102] Table 3 shows the electrochemical performance of various carbon-based SiOC composites.

A composite anode comprising graphene nanosheets and SiOC was synthesized by Ji and co-workers, and they were able to demonstrate a reversible discharge capacity better than that of graphite and monolithic SiOC.[116] These composite anodes exhibited an initial discharge capacity of 1141 mA h g^{-1}, but the discharge capacity decreased significantly after eight cycles to 364 mA h g^{-1}. Nevertheless, they have correlated the enhanced battery performance of these composite anodes to the formation of the new electrochemically active species, such as O_xSiC_y, at the interface between graphene and SiOC. Furthermore, their X-ray photoelectron spectroscopy studies also indicated the formation of inactive species like SiC_4, but in smaller quantities. It is interesting to observe that the discharge capacity has shown an almost linear increase (173 mA h g^{-1} to 357 mA h g^{-1}) with the increase in the weight fraction of graphene nanosheets (4 wt% to 25 wt%), although an optimum weight fraction of graphene nanosheets was not discussed.[116] Similarly, David and co-workers fabricated self-standing anodes consisting of silicon oxycarbide in a matrix of reduced graphene oxide to get the components' synergistic effect.[33] Reduced graphene oxide serves as a percolation network, which increases electrical conductivity, whereas amorphous SiOC particles increase lithium storage. The paper electrodes they developed have shown a storage capacity of ~588 mA h g^{-1} at the 1020th cycle. Another advantage of such paper-based electrodes is that they provide enormous flexibility and have great potential for developing flexible devices.[33,117] In another study, it was demonstrated that by embedding SiOC in graphite flakes, their electrical conductivity and structural stability can be significantly improved.[103] They have achieved a reversible storage capacity of 500 mA h g^{-1} after 1000 cycles. Their study also showed that in such systems, a significant improvement in diffusion coefficient can be achieved by shortening the Li-ion diffusion paths. A diffusion coefficient of 2.0×10^{-10} cm^2 s^{-1} was obtained, which is the highest value reported in the literature so far. Similar studies with carbon nanotubes have shown that a stable storage capacity of 686 mA h g^{-1} can be achieved at an average Coulombic efficiency of 99.6%.[108] It was also proposed that by nitrogen doping and by creating defects in carbonaceous fillers, it is possible to enhance the electrical conductivity and electrochemical performance.[13,111]

The previous discussion was on the external addition of carbonaceous materials. However, it is also possible to develop anode materials with better battery performance by *in situ* synthesis of carbon-containing silicon oxycarbide nanocomposites.[110] 1D-SiOC/C composite nanofibers synthesised *via* electrospinning and the pyrolysis route have a stable discharge

Table 2 Electrochemical performance details of SiOC ceramics as anode materials synthesised from various polymeric precursors and the temperature of pyrolysis

S. · no.	Specimen (current density mA g^{-1})	Synthesis temperature (°C)	Polymeric precursor	First reversible capacity (mA h g^{-1})	First cycle loss (%)	Reversible capacity (mA h g^{-1}) (after N cycles) (current density (mA g^{-1}))	Reference
1	SiO_2 rich dense SiOC. (18)	1400	Poly(methylhydrosiloxane)PHMS and 200% divinylbenzene (DVB)	241	60	0 (10 cycles)	Dibandjo *et al.* 2012 (ref. 24)
	HF etched porous SiOC (18)			268	58	Stable (30 cycles)	
2	Carbon rich SiOC–Ar (18)	1000	PHMS and 200%DVB	568	37	372 @ 2-C (50)	Pradeep *et al.* 2013 (ref. 91)
	Carbon rich SiOC–Ar/H_2 (18)			704	33	<200 @ 2-C (50)	
3	SiOC-PD2 (18.6)	1100	Polyramic RD-684a and DVB	603	39	200 @ 1-C (100)	Liu *et al.* 2013 (ref. 59)
4	PD2 (18)	1000	Low C= PHMS + TMTVS	656	41	600 (130)	Pradeep *et al.*
	PT2 (18)	1300	High C= PHMS + DVB	728	32	∼400 (130)	2014 (ref. 16)
5	SiOC (70)	1000	PHMS and DVB	862	26	—	Fukui *et al.* 2014 (ref. 17)
6	Carbon rich SiOC (360)	1000	PHMS and 200%DVB	650	47	600 (100)	Pradeep *et al.* 2015 (ref. 25)
7	PR/DVB 50/50 (37)	1000	Polyorganosiloxnes (RD-684a (PR),	504	36	338 (60)	Kaspar *et al.*
	PR (37)		RD-688 (RR), RD-212 (SR),	535	38	304 (60)	2016 (ref. 30)
	RR (37)		polysilsesquioxane PMS MK, and	434	39	255 (60)	
	SR/RR 50/50 (37)		DVB	501	38	237 (60)	
	SR/RR 25/75 (37)			682	42	91 (60)	
	Carbon rich SiOC						
8	SiOC–Ac/Ar (360)	900	PHMS and 200%DVB	763	49	570 (250)	Pradeep *et al.*
	SiOC Ac/H_2(360)			919	50	604 (250)	2016 (ref. 92)
	SiOC Cy/Ar(360)			332	65	307 (250)	
	SiOC Cy/H_2 (360)			495	48	477 (250)	
9	SiOC–Ar (36)	900	PHMS and 200%DVB	∼760	50	>400 (100)	Graczyk-zajac
	SiOC–CO_2 (36)			∼580	63	>200 (100)	*et al.* 2018 (ref. 84)
10	SiOC–P0 (72)	900	PSS-octakis(dimethylsilyloxy)				Lee *et al.* 2020
	SiOC–P1 (72)		substituted (POSS), PHMS, and				(ref. 83)
	SiOC–P2 (72)		DVB				
	SiOC–P2 (72)						
11	SiOC-DVB-1 (100)	1200	Polymethylsilsesquioxane (PMSQ)	819	35	476 (500)	Wu *et al.* 2022
	SiOC-DVB-2(100)		and DVB	929	36	463 (500)	(ref. 93)
	SiOC-DVB-3(100)			892	32	435 (500)	
	SiOC-DVB-4(100)			780	34	273 (500)	
12	SiOC–KF-54 (50)	900	KF-96 silicon oil and DVB	461	47	90% capacity retention in	Lim *et al.* 2021
	SiOC-105 (50)			412	47	all samples (500)	(ref. 58)
	SiOC-103 (50)			532	47		
	SiOC-101 (50)			829	38		
13	SiOC- PhTES (18.6)	1000	Phenyltriethoxysilane (PhTES)	652	39	80% capacity retention	Wilamowska
	SiOCPhTES : MTES 2 : 1 (18.6)		methyltriethoxysilane (MTES)	842	37	(140)	*et al.* 2014 (ref. 56)

Table 2 (*Contd.*)

S. no.	Specimen (current density mA g^{-1})	Synthesis temperature (°C)	Polymeric precursor	First reversible capacity (mA h g^{-1})	First cycle loss (%)	Reversible capacity (mA h g^{-1}) (after *N* cycles) (current density (mA g^{-1}))	Reference
	PhTES : MTES 1 : 1 (18.6)			939	39		
	PhTES : MTES 1 : 2 (18.6)			685	35		
	MTES (18.6)			303	75		
14	SiCO_Ph (50)	1000	PhTES, MTES & TEOS	538	49	—	Weinberger *et al.*
	SiCO_Ph_M (50)			745	33	—	2015 (ref. 94)
	SiCO_Ph_T (50)			858	27	400 @0.5 A g^{-1} (100)	
15	Me–SiOC (35)	1100	Methyltrimethoxysilane (MTMS;	761	47	241 (100)	Krüner *et al.*
	Vi–SiOC (35)		97%), vinyltrimethoxysilane	789	38	299 (100)	2018 (ref. 4)
	Vi-Ph-SiOC (35)		(VTMS; 99%), and	922	23	747 (100)	
			phenyltrimethoxysilane (PTMS; 97%				
16	PVA-SiOC (100)	900	PhTES and PVA	595	39	505 (150)	Shi *et al.* 2019
	P–SiOC (100)			533	54	235 (100)	(ref. 95)
17	H–SiOC-900 (50)	900	PhTES and TEOS	1115	25	961 (50), 480 @ 500 mA g^{-1} (200)	Xia *et al.* 2021 (ref. 96)
18	DDTS-SiOC (50)	800	1,5-Divinyl-3,3-diphenyl-1,1,5,5-	866	28	580 (50)	Mujib *et al.* 2021
	DTDS-SiOC (50		tetramethyltrisiloxane (DDTS),	800	48	800 (50)	(ref. 97)
	TPTS-SiOC (50)		1,3-divinyltetramethyldisiloxane (DTDS), and 1,3,5-trivinyl-1,1,3,5,5-pentamethyltrisiloxane (TPTS)	636	48	100 (50)	
19	SiOC-1000 (100)	800	1,3,5,7-Tetramethyl-1,3,5,7-	958	23	95% (60)	Raj *et al.* 2011
	SiOC-800 (100)		tetravinylcyclotertrasiloxane (TTCS)	906	33	100% (60)	(ref. 85)
20	SOC–HF (200)	950	1,3,5,7-Tetramethyl-1,3,5,7-	568	42	573@200 mA g^{-1}	Ma *et al.* 2016
	SOC (200)		tetravinylcyclotertrasiloxane (TTCS)	300	47	544@500 mA g^{-1} 233@200 mA g^{-1} 193@200 mA g^{-1} (100)	(ref. 63)
21	SiOC P_{1AC1} (37)	1000	Acenaphthylene	498	33	(40 (40)	Fukui *et al.* 2011
	SiOC P_{2AC1} (37)		$(Ph_2Si)_{0.85}(PhSi)_{0.15}$ and $(MePhSi)_{0.70}(Ph_2Si)_{0.15}(MeSi)_{0.15}$	580	32		(ref. 68)
22	SiOC PP-700 (74)	700–1200	Polystyrene	795	37	Improved@37 mA g^{-1} (30)	Fukui *et al.* 2013
	SiOC PP-900 (74)		Phenyl substituted polysilane	576	39	for all samples	(ref. 69)
	SiOC PP-1100 (74)		$(Ph_2Si)_{0.85}(PhSi)_{0.15}$	517	36		
23	SiOC-1100 (37)	1100	Polyramics RD-684 (SiOCRD684)	572	39	521@37 mA g^{-1} (75)	Kaspar *et al.*
	SiOC-1300 (37)	1300		374	43	367@37 mA g^{-1} (75)	2012 (ref. 88)
24	SiOC-1100 UV curing (37)	1100	Polyramics RD-684 (SiOCRD684)	658	39	630 (18.5) (350)	Kaspar *etal.* 2012 (ref. 27)
	SiOC-1300 UV curing (37)	1300		532	43	—	

Table 2 (*Contd.*)

S. no.	Specimen (current density mA g^{-1})	Synthesis temperature (°C)	Polymeric precursor	First reversible capacity (mA h g^{-1})	First cycle loss (%)	Reversible capacity (mA h g^{-1}) (after *N* cycles) (current density (mA g^{-1}))	Reference
25	SiOC (100)	900	Dimethylpolysiloxane,	676	—	800 @200 mA g^{-1} (250)	Halim *et al.* 2016
	Si/C composite (100)		poly(dimethylsiloxane-co-methylphenylsiloxane)			222 @200 mA g^{-1} (250)	(ref. 28)
26	SiCO_1.3 (50)	1000	Silicon tetraacetate	563	56	422 @ 200 mA g^{-1} (200)	Tahir *et al.*[98]
	SiCO_0 (50)		Citric acid	217	78		
27	SiOC BPO-C (50)	1000	4,40 -bis(triethoxysilyl)-1,10-biphenyl and triblock copolymer Pluronic P123	674	50	600 @ 50 Ma g^{-1} (200)	Weinberger *et al.*[29]
28	SiOC H44 (50)	1000	Methyl-phenyl-siloxane H44	578	46	~360 @100 mA g^{-1}	Mujib *et al.*[99]
	SiOC MK (50)		MK methyl-siloxane MK and	243	10	<100 for MK AND RSN	
	SiOC RSN (50)		phenyl-siloxane RSN	60	90	@100 mA g^{-1} (50)	
29	SiOC-500 (100)	500	Rose pollen grains and tetraethyl	578	43	351 (200)	Xia *et al.*[100]
	SiOC 600 (100)	600	orthosilicate (TEOS)	657	36	275 (200)	
	SiOC 700 (100)	700		284	55	220 (200)@100 mA g^{-1}	

capacity 70% higher than that of the Si/C nanofiber anodes. In this study, they achieved the necessary carbon content by adding polyacrylonitrile during the synthesis stage. It is to be noted that the requirement of adding carbon black or binders is unnecessary in such systems, thereby leading to better material usage.[110] In another study, the microstructure of the SiOC ceramics was modified with acenaphthylene to produce materials with a high C content. However, increasing the concentration of acenaphthylene also deteriorated battery performance due to the higher content of free carbon. An interesting phenomenon observed during delithiation is a pseudo-voltage plateau that needs to be explored further.[68]

In place of carbonaceous materials, other elements like tin and[124–127] antimony[128,129] and in some cases transition metal dichalcogenides based on $MoSe_2$ (ref. 130) were explored as active fillers for improving the overall battery performance of SiOC anodes. The addition of Sn and Sb enhances the battery performance of SiOC anodes due to their high electrochemical activity. In the case of Sn, it was found that its presence limits the formation of electrochemically inactive SiC domains in the material system. In contrast, the addition of Sb seems to modify the structure of SiC, creating more favourable sites. However, excessive addition of Sn or Sb particles may limit the performance due to the high volumetric expansion of Sn upon lithium insertion. Nevertheless, synthesising PDCs with excess free carbon could stabilise such systems.[127] Another primary concern with the addition of tin – especially in the case of *in situ* inclusion of Sn by carbothermal reduction of SnO_2 – is its consumption of free carbon during the synthesis process. This reduces the structural stability of such systems. Hence, to circumvent this problem, graphite particles can be added externally.[125] Evaluation of the effect of crystalline and amorphous silicon nanofillers on battery performance was conducted, and crystalline nanosilicon embedded systems were found to have a better storage capacity (905 mA h g^{-1}) than amorphous silicon embedded systems (704 mA h g^{-1}). However, amorphous silicon embedded systems deliver better performance when it comes to cycling stability. The nanosilicon particles under 10 nm are believed to have contributed to this better matrix integrity.[131] This paper also mentioned the possibility of improving the intrinsic electrical conductivity of nanosilicon-embedded systems due to the formation of SiC. However, such an improvement could potentially deteriorate battery performance because SiC is electrochemically inactive.[90] The electrochemical performance of various SiOC composites with non-carbonaceous fillers is presented in Table 4.

6.2 Enhancing the network connectivity between SiOC particles

The lack of an interconnected network between SiOC particles is a significant hurdle in fabricating these anode materials. By doping SiOC nanoparticles with boron, Zhu and co-workers demonstrated that an interconnected network of nanoparticles can be formed.[144] The boron acid coating on SiOC initially transforms into solid boron oxide at elevated temperatures. Subsequent thermal treatment beyond its glass transition

Table 3 Electrochemical performance of the carbon based SiOC composites

Specimen (current density mA g^{-1})	Synthesis temperature (°C)	First reversible capacity (mA h g^{-1})	First cycle loss (%)	Reversible capacity (mA h g^{-1}) (after N cycles) (current density (mA g^{-1})	Reference
Carbon based SiOC composites					
SiOC:C nanofiber (50)	700	839	27	669(80)	Li *et al.* (2014)[110]
SiOC:C nanohybrids (50)	800	436	46	470 (50)	Wang *et al.* 2016 (ref. 123)
SiOC/C NF-0.5(100)	1000	1011	32	707(200)	Huang *et al.* (2021)[13]
SiOC/PAN nanofiber (372)	1000	778	29	715(200)	Li *et al.* (2021)[109]
SiOC:CNT (100)	1000	948	35	846(40)	Shen *et al.* (2011)[107]
SiOC–CNT paper (8.5)		539.6	54		Bhandavat *et al.* 2011 (ref. 32)
SiOC–CNT-5 (0.1C)	1000	841	32	686 (40)	Bhandavat *et al.* 2013 (ref. 108)
Onion-like SiOC/C (100)	900	658	22	540 (50) 365 (500) 2 A g^{-1}	Lin *et al.* 2021 (ref. 35)
Graphite based SiOC composites					
GF-SiCO (93)	800	220	20	180 (350)	Saleh *et al.* 2016 (ref. 106)
SiOC/graphite (SG)(50)	1000	580	29	480 (1000) (0.5 A g^{-1} 184 (1000) (2 A g^{-1})	Wu *et al.* 2019 (ref. 103)
NCG@SiOC (372)	900	380	—	170 (100) @ 10-C (100)	Hong *et al.* 2020 (ref. 123)
	1100	520	28	300 @5-C, 200@10-C (1000)	
	1300	300	—	173 (100(10-C (100)	
$SiOC_{PhTES}/C2_g$ (186)	1000	472	40	214@5-C, 4230.5-C (20)	Knozowski *et al.* 2020 (ref. 104)
$SiOC_{PhTES}/C5_g$ (186)	1000	460	42	242@5-C, 4080.5-C (20)	
$SiOC_{PhTES}/C10_g$ (186)	1000	452	46	293@5-C, 3730.5-C (20)	
$SiOC_{VTES}/C2_g$ (186)	1000	730	30	519 (270)	Knozowski *et al.* 2021 (ref. 105)
$SiOC_{VTES}/C4_g$ (186)	1000	630	30	464 (270)	
$SiOC_{VTES}/C10_g$ (186)	1000	476	29	341 (270)	
Graphene oxide/reduced graphene oxide/graphene based SiOC composites					
LBL-SiOC-rGO (50)	800	780	—	400 (30)	Kolathodi *et al.* 2016 (ref. 113)
SiOC/rGO (100)	—	635	45	507(50)	Islam *et al.* 2016 (ref. 121)
SiOC@C/graphene(200)	950	674	38	691 (100) 676 (200)	Ma *et al.* 2022 (ref. 114)
[109]SiOC:exfoliated graphite	1000	530	54	357 (20)	Ji *et al.* (2009)[116]
10SiOC/graphene (50)	800	607	37	582 (90)	Ren *et al.* (2015)[115]
60SiOC (100)	1000	702	32	588 (1020)	David *et al.* 2016 (ref. 33)
3D GNS SiOC (100)	`1000	844	34	701(100)	Sang *et al.* 2018 (ref. 118)
3D GNS $SiOC_f$(100)	1000	929	21	775 (100)	Sang *et al.* 2020 (ref. 117)
NGA SiOC 25 (37)	900	747	33	605 (90)	Shao *et al.* 2020 (ref. 119)

temperature leads to the melting of boron oxide, which will penetrate the SiO_x species, forming a strong interfacial bonding. The robust coupling achieved because of this boron doping has enabled the fabrication of batteries with long life and high specific capacity at high current densities.[144] The schematic illustration of the assembly formation in B doped SiOC is illustrated in Fig. 5. Furthermore, the addition of boron nitride nanotubes (BNNTs) could affect free carbon evolution, which would result in improved electrochemical performance.[142] Adding 0.25 wt% BNNTs resulted in a first-cycle storage capacity of 812 mA h g^{-1}, which decreased with increasing BNNT weight fraction.

6.3 Introducing micropores into the ceramic matrix

The PDC route produces these ceramics, which are inherently porous due to the evolution of organic species. The porous anodes may not provide the best-performing anodes since porosity inherently reduces the active material, leading to low energy densities. However, pores, especially microsized ones, enhance the structural stability of these anodes due to their buffering capacity. Furthermore, it is also being observed that nanopores could ensure faster ion diffusion to the active sites of SiOC and provide more electrochemically active sites for lithium storage.[29,83] Such structural changes have resulted in high specific capacities of 980 mA h g^{-1} at a current density of 180 mA h g^{-1}.[83] In these systems, such high porosity levels and specific surface areas can be attained by etching with either KOH or HF.[63,64] However, excessive etching could also degrade battery performance.[64] By etching with HF, for instance, the Si–O active sites will be removed from the system, resulting in poor battery performance.

Table 4 Electrochemical performance of SiOC composites with non-carbonaceous fillers

Specimen (current density mA g^{-1})	Synthesis temperature (°C)	First reversible capacity (mA h g^{-1})	First cycle loss (%)	Reversible capacity (mA h g^{-1}) (after N cycles) (current density (mA g^{-1})	Reference
Si/SiOC composites					
Si/Si–O–C (50)	1100	1372	22	990 (30)	Liu *et al.* 2012 (ref. 132)
SiOC. N–Si-a (74)	1100	704	—	620(100)	Kaspar *et al.* 2014 (ref. 131)
SiOC. N–Si-c (74)	1100	905	—	314(50)	
Si@SiOC (100)	800	2093	29	2093 (200)	Choi *et al.* 2014 (ref. 133)
Si_{tc}:SiOC	1100	593	35	289 (50)	Vrankovic *et al.* 2016 (ref. 134)
Si_{tc}:30C:SiOC		533	39	575 (50)	
Si_s:SiOC		450	40	482 (50)	
Si_s:30C:SiOC		484	44	416 (50)	
Si/C/SiOC (18)	1100	2000		(100)	Vrankovic *et al.* 2016 (ref. 135)
Si/SiOC-0.6 (100)	800	980	37	800 (100)(100) 600 (100)(500) 480 (500)\(500)	Wu *et al.* 2019 (ref. 136)
Si–SiOC S-1 ()	—	2000	28	1750 (100)	Wei *et al.* 2020 (ref. 137)
Sn/SiOC composites					
$SiOC_{MK}$/Sn (37)	1000	566	52	232 (110)	Kaspar *et al.* 2014 (ref. 138)
$SiOC_{RD}$/Sn (37)		651	36	562 (110)	
1.1 Sn- SiOCfiber 1200(35)	1200	939	18	457 (100)	Tolosa *et al.* 2018 (ref. 127)
1.2 Sn– SiOC fibe1200 (35)		994	16	400 (100)	
SiOC/Sn-40 (18.6)	1000	756	26	549 (50)	Dubey *et al.* 2019 (ref. 124)
Sn@SiOC (100)	700	800	30	502 (300)	Shi *et al.* 2019 (ref. 139)
Sn@SiOC NPs (186)	900	656	33	411 (250)	Xia *et al.* 2020 (ref. 140)
Sn@SiOCNP (100)	600	918	27	~708 (200)	Wang *et al.* (ref. 141)
$SiOC:C_{0.2}$/Sn-40% (100)	1000	439	44	351 (100)	Knozowski *et al.* 2022 (ref. 125)
$SiOC:C_{0.2}$/Sn-60% (100)		507	38	441 (100)	
$SiOC:C_{0.1}$/Sn-60% (100)		512	37	378 (100)	
SiOC/Sn-40% (100)		572	35	521 (100)	
SiOC– SiO_2 hybrid spheres (100)	900	525	42	319 (100)	Shi *et al.* 2017 (ref. 61)
Bulk SiOC (100)		533	54	235 (100)	
SiOC spheres (100)		880	42	804 (100)	
Other (Sb, BNNT, MnO, and MoSe)/SiOC composites					
SiOC/Sb (18.6)	1000	667	41	507 (200) (372)	Dubey *et al.* 2020 (ref. 128)
SiOC–BNNT-0.25 wt% (100)	1000	410	50	237 (25) (1.6 A g^{-1})	Abbas *et al.* 2017 (ref. 142)
SiOC–BNNT-0.5 wt% (100)		250	58	47 (25) (1.6 A g^{-1})	
SiOC–BNNT-2 wt% (100)		317	54	82 (25) (1.6 A g^{-1})	
C/MnO/SiOC (100)	500	714	39	770 (200)	Huang *et al.* 2019 (ref. 143)
MnO/SiOC (100)		737	39	600 (200)	
SiOC/$MoSe_2$fiber mats	800	586	42	400 (100) (50 mA g^{-1})	Dey *et al.* (ref. 130)

In order to overcome etching issues, SiOC can be embedded in porous carbonaceous networks. Zhiyuan and co-workers infiltrated graphene sponge with a SiOC precursor and subsequently pyrolysed it to produce a hierarchical 3D interconnected structure of SiOC nanolayers wrapped in graphene sponge. Designing such hierarchical structures demonstrated improved electrical conductivity and ionic diffusivity.[118] In a similar study, Shao and co-workers also showed that fabricating graphene aerogel/SiOC heterostructures can improve the battery performance compared to unsupported silicon oxycarbide. They achieved a stable reversible charge capacity of 751 mA h g^{-1} with a Coulombic efficiency of ~99% after the first cycle.[119]

6.4 Fabricating thin film SiOC anodes

Thin films of SiOC are reported to perform better than their bulk counterparts.[106,144] At very high C rates, these thin-film SiOC anodes exhibited a reversible storage capacity of 1000 mA h g^{-1}. Thin films of these ceramics were fabricated by spray depositing the polymeric precursor on Cu, and then they were converted to a ceramic by pyrolysing them at 1000 °C. However, they have

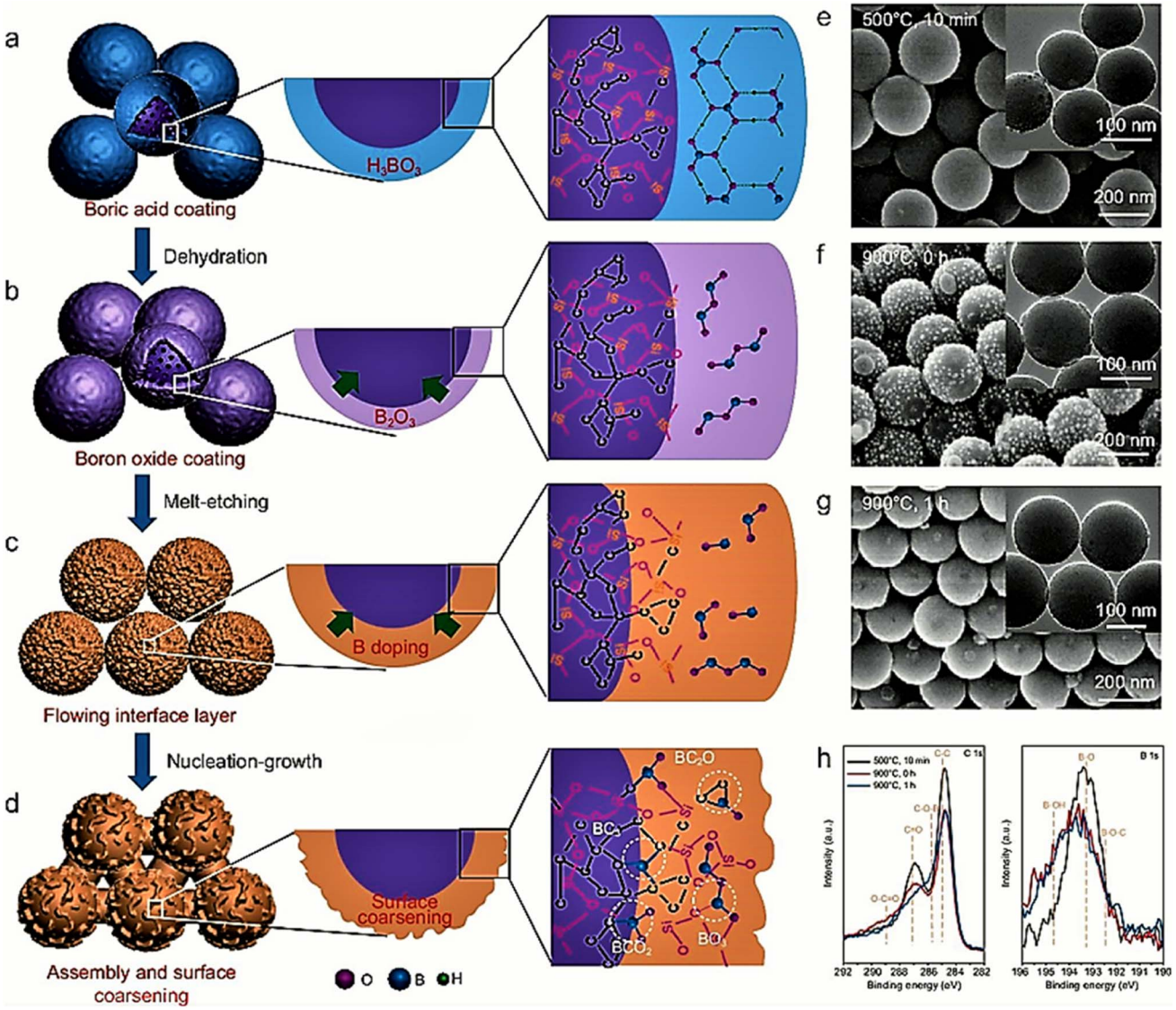

Fig. 5 (a–d) Schematic illustration of the assembly formation. (e–g) FESEM images of B–SiOC-2 at different reaction stages, and the insets are the corresponding TEM images. (h) C 1s and B 1s regions of the high-resolution XPS spectra of B–SiOC-2 at different reaction stages.[144] Reproduced with permission from ref. 144. Copyright 2020, Oxford University Press.

noticed that beyond a thickness of 1 μm, these films get peeled out of the Cu substrate due to the volumetric changes occurring during lithium cycling.[144] In another study by Wei and co-workers, thin film anodes of Si/SiCO exhibiting reversible capacities of 2000 mA h g^{-1} were reported.[137] They achieved such exceptional recharge capacities due to the presence of nano-silicon. First principles studies on such systems revealed that the small size voids, less than 1 nm, present in Si–C/O tetrahedra create a suitable environment for lithium-ion insertion.[137]

6.5 Synthesizing SiOC anodes with a spherical morphology

Using another exciting strategy, SiOC with spherical morphology has been synthesized in order to improve the performance of anodes.[2,61,94] Such systems have shown a stable reversible capacity of ~900 mA h g^{-1} at a current density of 100 mA g^{-1} with a Coulombic efficiency of ~98%.[61] These SiOC spheres are typically synthesised by a sol–gel process followed by carbonisation in an Ar atmosphere. Other methods, such as emulsion templating, were also utilized to synthesize spherical SiOC microbeads with hard and dense surfaces.[2] The porous interior structures of these microbeads could also account for the faster diffusivity of Li ions (4.5×10^{-6} cm^2 s^{-1}), and eventually lead to better performance. Interestingly, such systems exhibited a high first-cycle Coulombic efficiency of ~73% compared to other SiOC systems (~50% or less).[94]

6.6 Modifying the synthesis route

Several alternative processing strategies have been reported for synthesising SiOC ceramics, and the processing parameters significantly affect battery performance. One such technique

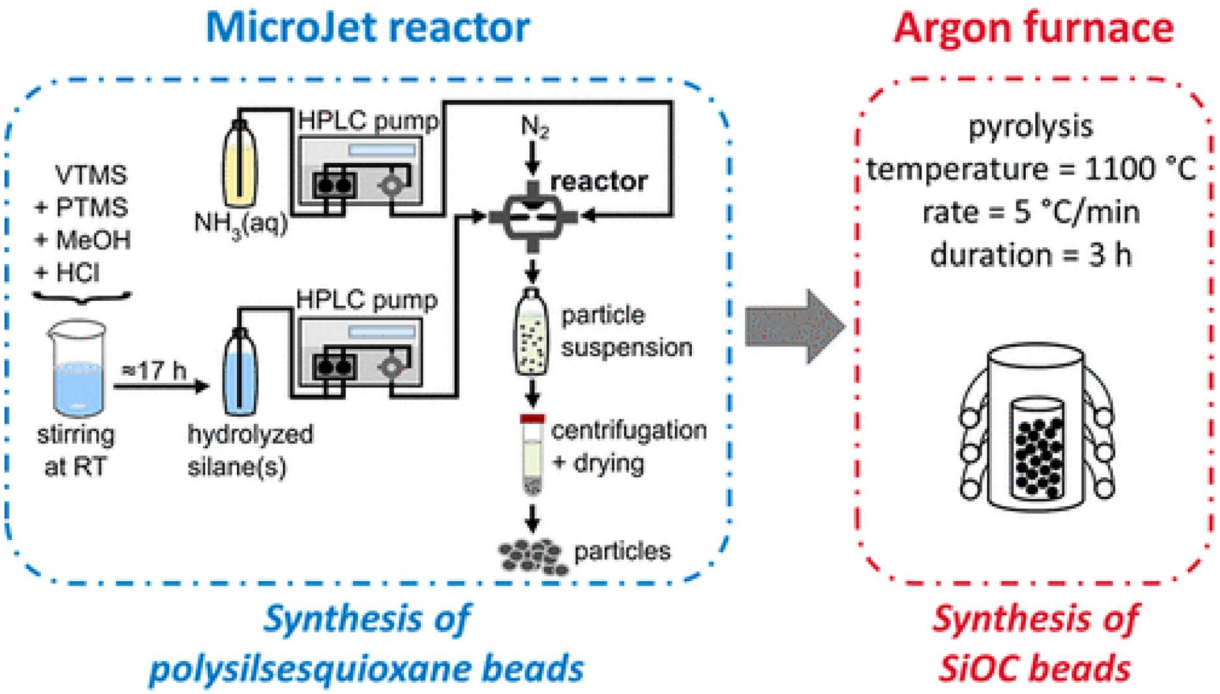

Fig. 6 Schematic synthesis using a microjet reactor to obtain polysilsesquioxane beads transformed into silicon oxycarbide beads *via* thermal treatment in argon.[4,145] Reproduced with permission from ref. 145. Copyright 2018, American Chemical Society.

involves mixing silicon tetraacetate with citric acid and thermally treating it at 250 °C. Subsequently, the solid material is carbonised in an Ar atmosphere. Detailed characterisation using X-ray photoelectron spectroscopy revealed the presence of oxycarbide species. The galvanostatic charge/discharge experiments on such systems showed a capacity of 590 mA h g^{-1} at 50

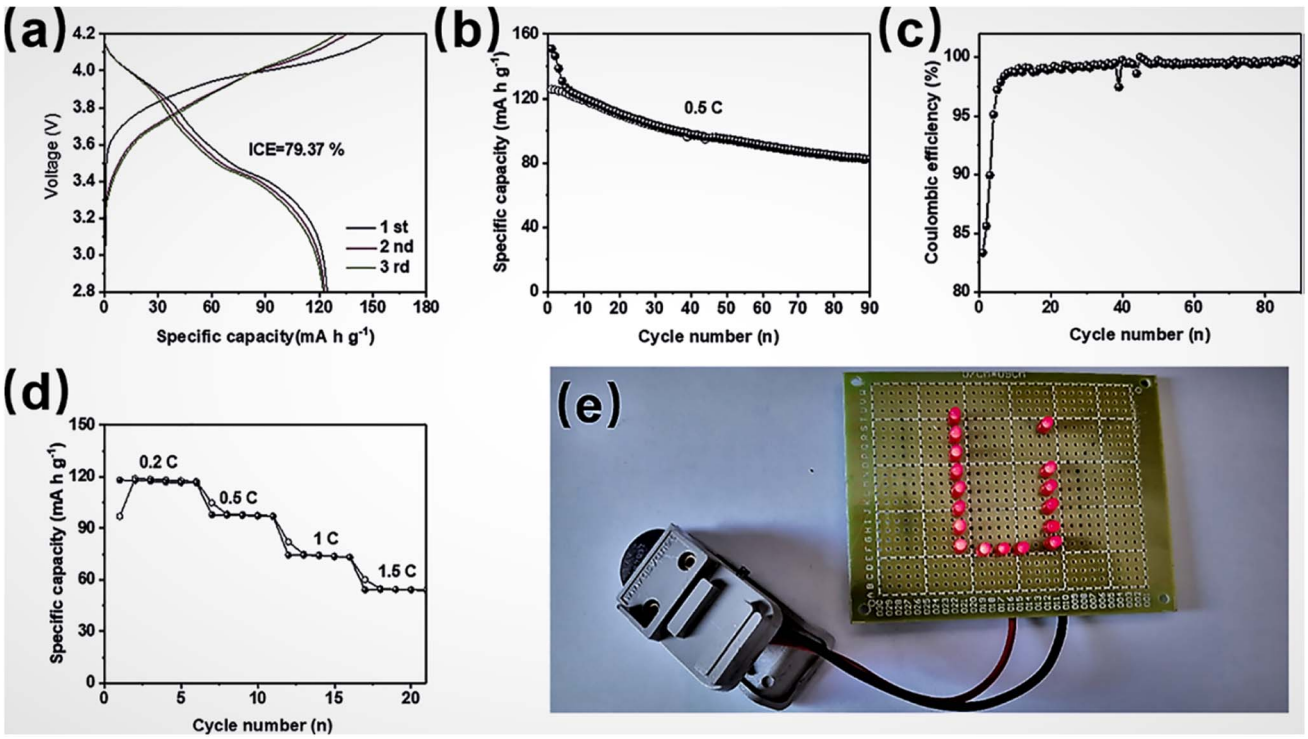

Fig. 7 (a) Voltage profiles for the first three cycles at 0.4C, (b) cycling performance, (c) Coulombic efficiency at 0.5C, and (d) rate performance of the as-assembled (−)pre-SiOC/C||LCO(+) full cell, and (e) the digital image of an LED bulb array lit up by the as-assembled (−)pre-SiOC/C||LCO(+) full cell.[35] Reproduced with permission from ref. 35. Copyright 2020, Elsevier.

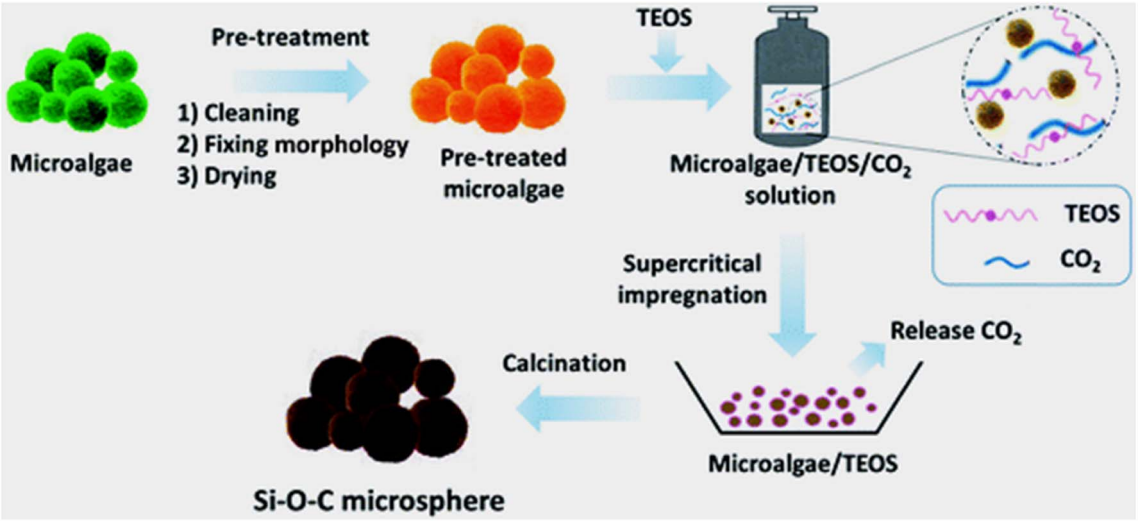

Fig. 8 Schematic illustration of the preparation process of SiOC microspheres based on bio-templating methods with the assistance of supercritical CO_2 fluid.[150] Reproduced with permission from ref. 150. Copyright 2016, Royal Society of Chemistry.

mA g^{-1}. Furthermore, in this study, a prelithiation step has been carried out to improve the reversible capacity.[98] Krüner and co-workers demonstrated the significance of choosing a continuous microjet reactor technique for producing large quantities of SiOC (Fig. 6). In this study, different types of alkoxysilanes were used. Among these, a mixture of vinyl and phenyltrimethoxysilane was identified as the best-performing material with a reversible storage capacity of 922 mA h g^{-1}.[4]

6.7 Prelithiation

The low initial Coulombic efficiency (ICE) is one of the major constraints that limit the practical application of SiOC.[61,69,118] To overcome the challenge of lower ICE, several prelithiation strategies have been proposed in the literature, including electrochemical prelithiation, chemical prelithiation, and doping using prelithiation agents.[146,147] Among these techniques, the electrochemical prelithiation technique is widely employed, but scaling it for applications is a challenge.[148] X. Lin and co-workers proposed an *in situ* chemical prelithiation technique by injection pyrolysis of lithium hepta(i-butyl) silsesquioxane-trisilanolate to produce cells with high ICE.[35] Li_xSiO_y will be formed *in situ* during the pyrolysis of the precursor, thereby reducing the consumption of Li ions in the initial cycles leading to high ICE. Furthermore, the onion-like structure formed during the synthesis is capable of buffering the large volumetric strain during repeated cycling (Fig. 7).

6.8 Bio-templating method

In another novel strategy for the synthesis of SiOC ceramics, microalgae-based on *Nannochlropsis*[149] and *Chlorella*[143] were used as bio-templates (Fig. 8). In another interesting study, rose pollen was considered the bio-template and carbon source.[100] Furthermore, supercritical CO_2 fluid was used as the solvent since this was found to ensure efficient mass transfer and uniform dispersion of precursors. By following this route, Xia and co-workers could produce SiC_nO_{4-n} species embedded in an amorphous carbonaceous network, thereby enabling a reversible charge capacity of 450 mA h g^{-1} at a current density of 0.1 A g^{-1} with an excellent Coulombic efficiency of ~100%.[150] In a *Chlorella*-based system, Huang and co-workers demonstrated that by embedding MnO nanoparticles in the SiOC matrix, a stable reversible capacity of 770 mA h g^{-1} at 100 mA g^{-1} can be achieved.[143] These studies suggest that it is possible to achieve high storage and cycle retention capabilities by tailoring the morphologies and microstructures of SiOC.

7. Mechanical properties

The SiOC based anode materials are rarely examined for their mechanical properties in the literature. From our literature survey we can find only one study in which uniaxial tensile tests were conducted on paper electrodes embedded with SiOC in a reduced graphene oxide matrix.[122] They used custom-built equipment to perform the uniaxial tensile tests (Fig. 9a–e). The reduced graphene oxide sample exhibited a strength of ~10.7 MPa at a failure strain of 2.8%, whereas the silicon oxycarbide (60 wt%) embedded reduced graphene oxide sample exhibited a tensile strength of ~2.7 MPa at a failure strain of 1.1%. The reported strains to failure are significantly large, indicating that the anodes can accommodate enormous volumetric strain. Furthermore, they noticed the presence of microfeatures on the surface of the anode after the tensile test. Interestingly, the fracture modes in reduced graphene oxide paper and the composite paper differed distinctly. The reduced graphene oxide paper has suddenly failed with a crumpled crack surface, whereas the cracked surface was sharp in the composite paper.[122]

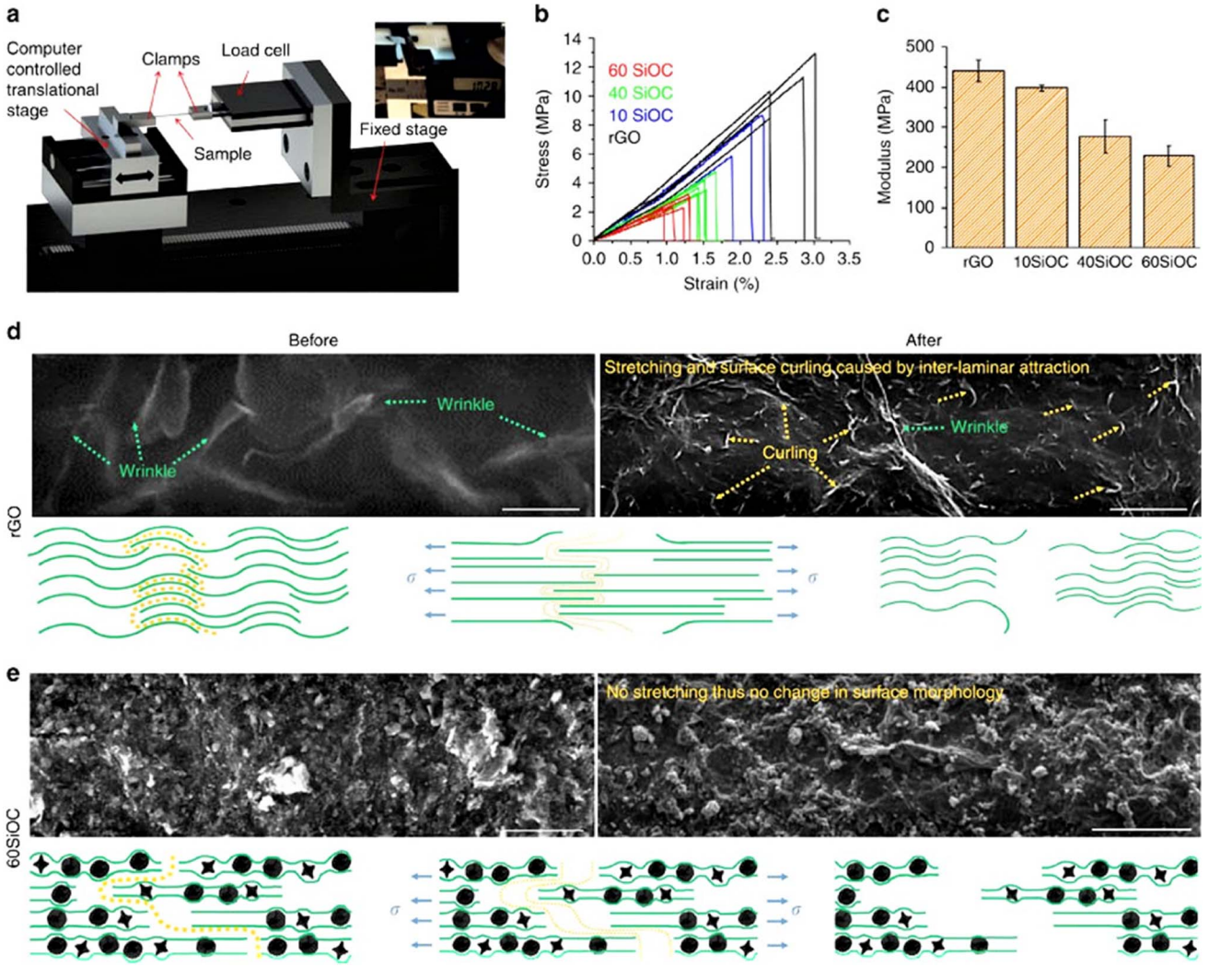

Fig. 9 (a) Schematic of the tensile testing setup with a photograph of rGO paper immediately after the fracture. The scale reading in the photograph indicates the length change to be ~0.28 mm. (b) Engineering stress *versus* strain plots of various freestanding papers derived from load *versus* displacement data, and (c) their corresponding modulus values. Error bars are 26.8, 7.6, 41.5, and 24.1 MPa for rGO, 10SiOC, 40SiOC, and 60SiOC, respectively. The SEM images and schematic illustration show the predicted fracture mechanism in rGO and 60SiOC freestanding papers: (d) The rGO paper experienced stretching and rearrangement of graphene sheets before failure. (e) For 60SiOC paper, negligible stretching or rearrangement occurred. The fracture line follows SiOC particles embedded in rGO flakes, resulting in gradual separation/tearing of the paper. The scale bar is 20 μm in all images.[122] Reproduced with permission from ref. 122. Copyright 2016, Springer Nature.

8. Other electrochemical applications

8.1 Enhancing the electrochemical performance of Si-anodes

Silicon has a very high theoretical capacity of (~4200 mA h g^{-1}), ~10 times that of graphite. However, as discussed above, due to high volumetric expansion (~300%), it is challenging to envisage Si as an effective anode material. One way to overcome this constraint is to synthesize silicon particles embedded in a SiOC matrix.[101,131,133] By embedding Si nanoparticles in an amorphous SiOC matrix, the extreme volumetric strain experienced by the silicon particles can be suppressed, and the free carbon present in the matrix can act as a good electrical conductor. One method by which it is synthesised is the selective assembly method, and by effectively using surfactants such as cetrimonium bromide (CTAB), interfacial interactions between silicon nanoparticles and silicon oil can be ensured. Such studies have shown a stable capacity of 1312 mA h g^{-1} for 100 cycles at 0.5 A g^{-1} (Fig. 10).[101]

In another method, Si nanoparticles were coated with suitable polymeric precursors, and then pyrolysed to synthesise SiOC-embedded Si particles. These SiOC-embedded systems resulted in the fabrication of fracture-free silicon anodes having a reversible capacity of 2093 mA h g^{-1} with a Coulombic efficiency of 92% after 200 cycles.[133] Their transmission electron microscopy studies reveal that the silicon oxycarbide-coated Si anodes are more robust than traditional graphite-coated Si anodes. This study has achieved coating by a scalable spray pyrolysis process. The coating was stable since the SiOC glass phase can expand during lithiation and therefore accommodate

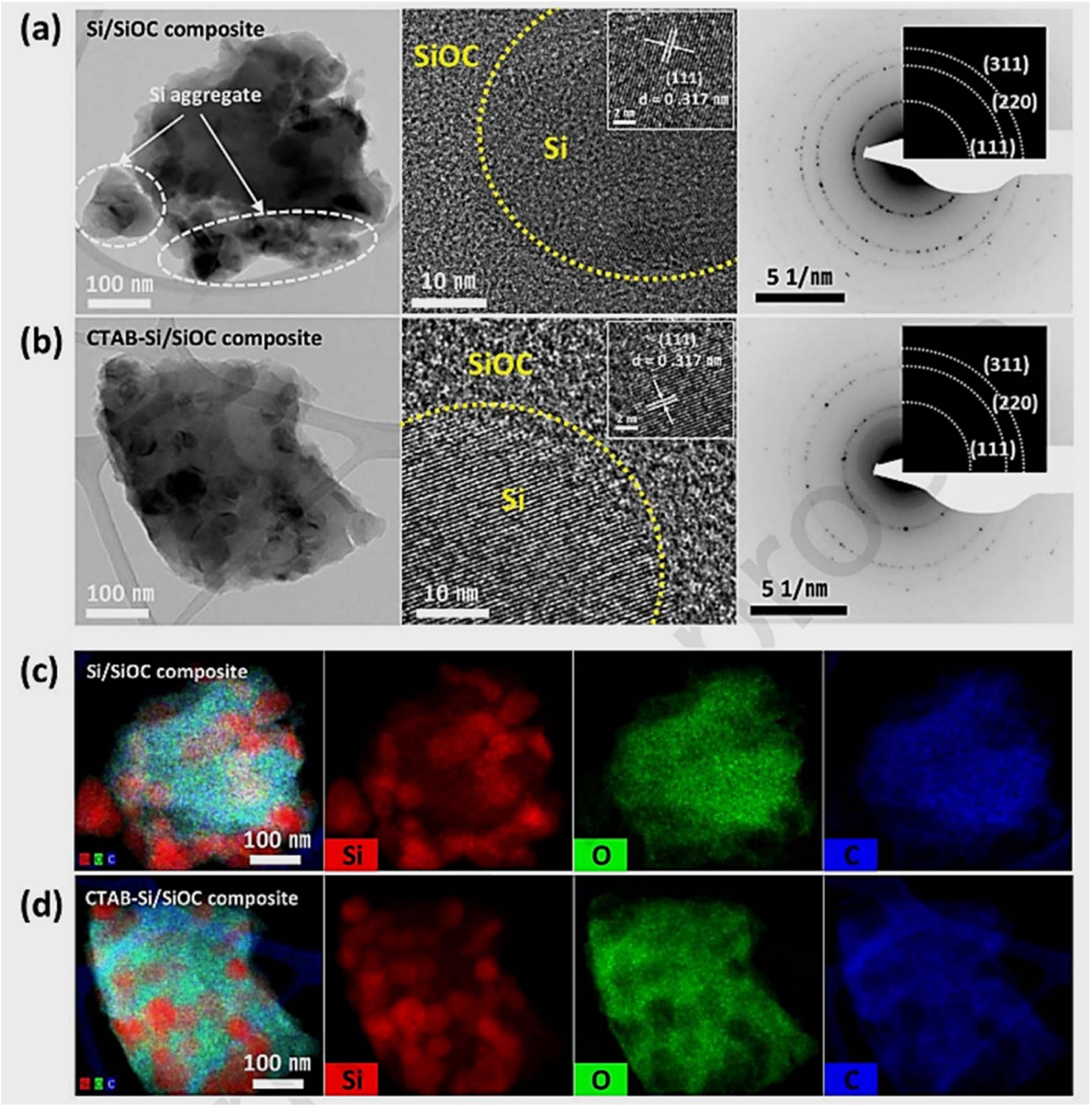

Fig. 10 Low-magnified TEM images, HR-TEM images with the inset showing the lattice fringes of Si, and SAED patterns of (a) Si/SiOC and (b) CTAB-Si/SiOC composites. EDS mapping of (c) Si/SiOC and (d) CTAB-Si/SiOC composites including elemental Si, O, and C.[101] Reproduced with permission from ref. 101, Copyright 2020, Elsevier.

the volumetric strain of the inner silicon nanoparticles. Furthermore, the SiOC phases act as a bridge between silicon nanoparticles, thereby improving structural integrity. However, the optimum thickness required to achieve the required capacity has not been discussed in this study.

8.2 Lithium–tin anodes

SiOC materials were also explored to improve the structural integrity of lithium–tin anodes. A tin-based anode has a reversible storage capacity of 994 mA h g^{-1}, which is about three times higher than that of a graphite anode.[14] However, similar to Si anodes, these materials expand significantly (~260%) during lithiation, thereby leading to poor structural integrity. Several efforts toward developing stable Sn anodes resulted in the development of Sn anodes dispersed in a SiOC matrix. Kaspar and group synthesised SiOC/Sn nanocomposites by chemically modifying the polysiloxane precursors (C-rich and C-lean) with tin acetate.[138] The Sn nanoparticles were 10 to 45 nm in size. Their studies revealed a first-cycle storage capacity of 651 mA h g^{-1} for the C-rich precursor-based system. They hypothesised that the excess C present in these systems is responsible for

accommodating the volumetric strain, thereby leading to better structural integrity. Furthermore, they have also observed a dependency of the type of Li–Sn alloy formation on the composition of SiOC. In the C-rich system, Li_7Sn_2 was observed, whereas for the C-lean system, $Li_{22}Sn_5$ was observed. However, achieving homogeneous distribution of Sn nanoparticles in the matrix was difficult in these systems leading to relatively lower cycling stability. The presence of highly ordered C further limited its reversible storage capacity. Hence, Dubey and co-workers synthesised SiOC/Sn nanocomposites to overcome these challenges by chemically modifying polysiloxane precursors with tin ethyl hexanoate.[124] By choosing tin ethyl hexanoate instead of tin acetate, they could achieve better homogeneity in the matrix. Moreover, the excess carbon observed in these new systems was highly disordered yielding storage capacities of 553 mA h g^{-1} at a current density of 2232 mA h g^{-1}. Furthermore, the scanning transmission electron microscopy studies of the samples that are cycled after 180 cycles revealed insignificant pulverisation, demonstrating the high structural stability of these composite systems.[124]

8.3 Sodium-ion batteries

In light of the wide availability of sodium, rechargeable sodium-ion batteries are considered an alternative to lithium-ion batteries. However, sodium ions have a much larger size than lithium ions, resulting in severe volumetric fluctuations during charging and discharging. The density of sodium is higher (0.97 g cm^{-3}) than that of Li ions (0.53 gcm^{-3}), which makes it heavier. The ionic radius of a Na ion is also much larger than that of a Li ion which may lead to low packing density and severe volumetric strain. Therefore, the efforts are towards developing suitable anode materials to accommodate sizeable volumetric strain. Several studies have shown that 2D materials such as MoS_2, because of its large inter-layer spacing of 0.62 nm, can act as a good host for sodium ions.[151–153] However, due to its low electrical conductivity and structural instability, capacity fading seems severe in MoS_2-based systems. H. Lim and co-workers have shown that by encapsulating MoS_2 in SiOC, it is possible to improve the structural stability of MoS_2. Furthermore, to improve the electrical conductivity, they have performed nitrogen doping of MoS_2. The core–shell structures resulted in high storage capacities of 540.7 mA h g^{-1} and these structures are reported to exhibit excellent capacity retention for more than 100 cycles.[154] Similar to MoS_2, antimony is also a suitable candidate anode material for sodium-ion batteries. It has a theoretical capacity of 660 mA h g^{-1}. However, its practical utility is limited because of its high volumetric expansion and sluggish kinetics. Hence, like MoS_2, Lee and co-workers embedded Sb in a silicon oxycarbide matrix and demonstrated a storage capacity of 510 mA h g^{-1}. Moreover, the capacity is retained for 250 cycles at 97% efficiency, even at a high current density of 20C.[155] These studies show that encapsulating the active material in amorphous SiOC can improve the structural stability of these anode materials.

Interestingly, SiOC synthesised from silicone oils was also directly explored as an anode material in sodium-ion batteries. Their cell capacities were somewhat limited to 160 mA h g^{-1} at 25 mA g^{-1} for 200 cycles. Nevertheless, the stability of such systems was exceedingly high – 00.09 mA h g^{-1} decay per cycle for 650 cycles.[156] Since the overall capacities are very low, strategies such as increasing the amount of carbon-rich SiOC phases and decreasing the presence of inactive sites such as SiO_2, SiC and free carbon phases were explored by other researchers.[157] Moreover, detailed structural studies using X-ray

Table 5 The electrochemical performance of sodium-ion batteries employing polymer derived SiOC and various SiOC-based composites as anodes

Specimen (current density mA g^{-1})	Synthesis temperature (°C)	First reversible capacity (mA h g^{-1})	First cycle loss (%)	Reversible capacity (mA h g^{-1}) (after N cycles) (current density (mA g^{-1})	Reference
SiCO_Ph (25)	1000	83	70	—	Weinberger *et al.*[94]
SiCO_Ph_T (25)		188	53	150 (40)	
SiOC/HC_G (37)	1000	201	35	141 (50)	Kaspar *et al.*[160]
SiOC(N)/HC_G(37)	1000	110	49	105 (50)	Kaspar *et al.*[160]
SiOC/HC_{PS}(37)	1000	140	45	67(50)	Kaspar *et al.*[160]
SiOC(N)/HC_{PS}(37)	1000	56	67	42 (50)	Kaspar *et al.*[160]
Sb/SiOC (18.6)	900	510	32.4	480 (250) (74)	Lee *et al.*[155]
900C-1h-10M (25)	900	189	57	160 (200)	Chandra *et al.*[156]
SiOC (20)	1000	175	63	100 (500)	Dou *et al.*[158]
SiOC-(BPO–C) (50)	1000	226	62	166 (10) decreased drastically after 90 cycles	Weinberger *et al.*[29]
SiOC-1300 (25)	1300	210	70	125 (600)	Chandra *et al.*[159]
HFC-Sb/SiOC (33)	900	403	34.5	344.5 (150) (0.2-C)	Kim *et al.*[129]
LFC-Sb/SiOC (33)	900	376	34.5	217 (150) (0.2-C)	
SIOC with FEC (25)	900	226 (10)	54	191.7 (20)	Putra *et al.*[161]
SIOC without FEC (25)	900	184 (10)	60	—	
MoS_2–SiOC (25)	800	199	30	190 (100)	Soares *et al.*[153]
N–MoS2/C@SiOC	900	540.7	24.5	~692(200)	Lim *et al.*[154]
SiOC (DS-N2-1) (25)	900 then 1300	234	41.5	160 (140)	Chandra *et al.*[157]
HC-SIOC-1(50)	1200	295	34	260 (50)	Cheng *et al.*[162]

Table 6 The electrochemical performance of SiOC materials employed as supercapacitors

Specimen & (current density)	Synthesis temperature	Capacitance ($F\ g^{-1}$)	Electrolyte	Specific surface area ($m^2\ g^{-1}$)	Capacity retention % (no of cycles)	Reference
SiOCDC-1 (30 $A\ g^{-1}$)	1000	110	1 M TEABF4 in acetonitrile	~2000	95% (10 000)	Meier *et al.* 2014 (ref. 165)
SiOC-DC (1 $A\ g^{-1}$)	1000	148.7	5 M KOH aqueous solution	2635	94.3% (2000)	Duan *et al.* 2015 (ref. 166)
SiOC-CDC (0.1 $A\ g^{-1}$)	1200	135	1 M tetraethylammonium tetrafluoroborate in acetonitrile	2394	86% (10 000)	Tolosa *et al.* 2016 (ref. 167)
SiOC (4.5 $A\ g^{-1}$)	900	—	1 M $LiPF_6$ in a 1 : 1 : 1 v/v mixture of EC/DMC/EMC	3.2	90% (75 000)	Halim *et al.* 2017 (ref. 164)
LBL-SiOC-rGO (6.7 $A\ g^{-1}$)	800	75.72	6 M KOH aqueous solution	—	56.13 (464)	Kolathodi *et al.*[113]
SiOC 0.5 wt% BNNT(1 $A\ g^{-1}$)	1000	78.93	6 M KOH aqueous solution	—	86% (185)	Abbas *et al.* 2017 (ref. 142)
SiOC SSCs (5 $mV\ s^{-1}$)	900	141	1 M Li_2SO_4	5.64	86.2	Pazhamalai *et al.* 2020 (ref. 168)
		115	1 M $TEABF_4$		92.8 (5000)	
SiOC H44 fibers	1000	50	1 M aq. Na_2SO_4	278.2	100 (2000)	Mujib *et al.* 2020 (ref. 99)
SiOCmkfibers		30				
SiOCRSNfibers (100 $mV\ s^{-1}$)		20				
NSDC NiO-10 (1 $A\ g^{-1}$)	300	804	3 M KOH	899	73.2 (5000)	Pan *et al.* 2021 (ref. 163)
SiC/SiOC/C (1 $mA\ cm^{-2}$)	1500	27.2 $mF\ cm^{-2}$	2 M KCl	—	90 (1000)	Okoroanyanmu *et al.* 2021 (ref. 169)
TPTS SiOC (2 $mV\ s^{-1}$)	800	78 (474 $mF\ cm^{-2}$)	1 M H_2SO_4	235	100 (5000)	Mujib *et al.* 2021 (ref. 97)
NHXF (20 $mV\ s^{-1}$)	1000	333	6 M KOH	1798	—	Swain *et al.* 2022 (ref. 170)
TRP13F24 (0.1 $A\ g^{-1}$)	1300–1400	225–165	1 M H_2SO_4	550	—	Mazo *et al.* 2022 (ref. 171)

photoelectron and nuclear magnetic resonance spectroscopy have revealed interesting results in these systems.[158] They have selected two techniques for the analysis, one involving etching with HF having considerably high porosity levels and the other which does not involve etching. Comparison between the two indicated that SiOC acts as active sites for sodium, but the mechanism seems to not be an alloying mechanism. Instead, due to the initial sodium intake, an irreversible structural change occurs, contributing to sodium intake. Furthermore, systematic studies toward understanding the mechanism of sodium intake in SiOC ceramics were carried out with *exsitu* measurements and DFT calculations.[159] Based on the various *ex situ* analyses, they concluded that sodiation up to 0.4 V occurs mainly in the carbon-rich SiOC phase and the micropores, whereas at voltages between 0.4 and 0.1 V, silicon-rich sites were activated for sodiation. However, at voltages below 0.1 V, sodium ions tend to react with amorphous Si to form silicon-rich compounds. Interestingly, SiC sites seem to contribute significantly to the cycling stability up to 6000 cycles at 200 mA g^{-1}.[159] The details of the electrochemical performance studies on sodium-ion batteries employing SiOC and SiOC-based composites as anodes are presented in Table 5.

8.4 Supercapacitors

Supercapacitors fabricated from SiOC ceramics were also investigated. Using electrospinning and pyrolysis, SiOC fibre mats were prepared from three preceramic polymers (MK, H44, and RSN) and evaluated for specific capacitance. Due to the higher concentration of free carbon in H44 (methyl-siloxane), electrodes prepared from this material showed the best performance with a specific capacitance of 50 F g^{-1} and capacity retention of 100% for 2000 cycles.[99] Moreover, NiO loaded on Ni–S doped silicon oxycarbide (NSCDC) exhibited excellent cycling properties and exhibited a capacitance of 804 F g^{-1} at 1 A g^{-1}. It was achieved by NSCDC's excellent electrical conductivity and its hierarchical porous structure, which enhanced ionic and electronic transport.[163] Surprisingly, an ultra-low carbon-SiOC ceramic synthesized by pyrolyzing a silicone oil rich in phenyl was found to be effective for LIBs because of its low reversible storage capacity (238 mA h g^{-1}). This exhibited pseudocapacitor properties in the voltage range of 0–1 V *versus* Li/Li^+.[164] The electrochemical performance details of SiOC materials employed as supercapacitors in the literature are tabulated in Table 6.

9. Summary and perspectives

The use of PDC-based materials is expected to have a significant impact on the development of high-capacity, energy-efficient batteries and supercapacitors. Hence, as we have seen through this review, silicon oxycarbides as anode materials in lithium ion batteries are widely explored. Due to their amorphous and porous nature, they have an electrochemical storage capacity almost double that of graphite anodes. As discussed in this review, we have highlighted the various factors that affect electrochemical performance, the significance of first-principles studies, as well as strategies for overcoming the inherent challenges.

In spite of recent progress, there are still scientific issues to be resolved to ensure their commercial viability. Identifying a precursor that would provide the best electrochemical performance is one of the major challenges. For the synthesis of SiOC anodes, several types of precursors have been reported in the literature. These factors result in a wide range of energy storage values from 200 to 1300 mA h g^{-1}. A number of SiOC ceramics have high storage capacities, but they tend to be poorly cyclable anodes. In some other systems, however, the reverse is true. It is therefore essential to have a deeper understanding of precursor chemistry in order to fabricate cells that are capable of meeting the demands of industrial applications. We suggest implementing a standardized synthesis procedure for SiOCs to ensure better repeatability. Furthermore, it is important to ensure the proper selection of precursors that guarantee a ceramic yield of more than 90% to ensure commercial viability. A higher ceramic yield not only ensures low volatile emission during synthesis but also enhances the environmental friendliness of these sytems.

To gain deeper insights into mechanisms causing irreversibility and capacity fading in SiOC systems, invasive characterisation techniques should be used after cycling or after lithiation. A combination of first principles and computational studies as well as machine learning techniques may be applied to determine the best precursor chemistry. Electrochemical characterisation studies should be conducted according to standard testing protocols to assess cell performance, such as current density, C-rate, rate capability, *etc.*, so that proper comparisons between different SiOC systems can be made.

In contrast to Si-anodes that are widely researched, SiOC anodes and their interactions with various other cell components such as current collectors, electrolytes, and binders are less well explored and understood. A number of additives have been explored, and graphene is one of the most prominent. Research should be conducted to develop conductive binders and additives for electrolytes in order to increase the energy density of these batteries. For practical applications, it is crucial to have a homogeneous distribution of the PDC material in the electrode. In addition, the role of particle size and distribution in the electrochemical properties is unclear. According to previous studies, the interface between the SiOC electrode and the Cu current collector is improper, which results in inefficient energy transfer. The use of alternative current collectors such as Bucky papers could ensure a proper interface.[172] Furthermore, the fabrication of these anodes should take advantage of advances in recent fabrication techniques, including lithography and additive manufacturing. The mechanical stability and safety of the device are other aspects that are crucial for determining their suitability for practical applications. As far as we know, there has not been a detailed study on this topic. Despite SiOC anodes' advantages over their counterparts such as Si and graphite anodes, they are still a long way from commercial viability for large-scale applications.

Conflicts of interest

The authors declare that they do not have any conflicts of interest.

Acknowledgements

The authors would like to acknowledge HBL Power Systems Limited for funding the project related to Li-ion batteries and providing access to various research facilities in their R&D lab. This work was partially supported by the US National Science Foundation EPSCoR Program under NSF Award # OIA-1655740. The US National Science Foundation Graduate Research Fellowship Program GRFP (DGE-1744593) also provided additional support for Michelle Greenough. However, the views, conclusions and recommendations expressed in this material are those of the author(s) and do not necessarily reflect those of the US National Science Foundation.

References

1 B. Diouf and R. Pode, *Renewable Energy*, 2015, **76**, 375–380.
2 B. Dong, Y. Han, T. Wang, Z. Lei, Y. Chen, F. Wang, H. Abadikhah, S. A. Khan, L. Hao, X. Xu, R. Cao, L. Yin and S. Agathopoulos, *ACS Appl. Energy Mater.*, 2020, **3**, 10183–10191.
3 H. Li, Z. Wang, L. Chen and X. Huang, *Adv. Mater.*, 2009, **21**, 4593–4607.
4 B. Krüner, C. Odenwald, N. Jäckel, A. Tolosa, G. Kickelbick and V. Presser, *ACS Appl. Energy Mater.*, 2018, **1**, 2961–2970.
5 Md. A. Rahman, G. Song, A. I. Bhatt, Y. C. Wong and C. Wen, *Adv. Funct. Mater.*, 2016, **26**, 647–678.
6 S. Chen, L. Shen, P. A. van Aken, J. Maier and Y. Yu, *Adv. Mater.*, 2017, **29**, 1605650.
7 J. E. Entwistle, G. Beaucage and S. V. Patwardhan, *J. Mater. Chem. A*, 2020, **8**, 4938–4949.
8 C. Jiang, L. Xiang, S. Miao, L. Shi, D. Xie, J. Yan, Z. Zheng, X. Zhang and Y. Tang, *Adv. Mater.*, 2020, **32**, 1908470.
9 M. Ge, C. Cao, G. M. Biesold, C. D. Sewell, S. Hao, J. Huang, W. Zhang, Y. Lai and Z. Lin, *Adv. Mater.*, 2021, **33**, 2004577.
10 Y. Qi, G. Wang, S. Li, T. Liu, J. Qiu and H. Li, *Chem. Eng. J.*, 2020, **397**, 125380.
11 X. Zuo, J. Zhu, P. Müller-Buschbaum and Y.-J. Cheng, *Nano Energy*, 2017, **31**, 113–143.
12 B. Liang, Y. Liu and Y. Xu, *J. Power Sources*, 2014, **267**, 469–490.
13 X. Huang, B. Christopher, S. Chai, X. Xie, S. Luo, S. Liang and A. Pan, *ACS Appl. Energy Mater.*, 2021, **4**, 1677–1686.
14 W.-J. Zhang, *J. Power Sources*, 2011, **196**, 13–24.
15 M. Ashuri, Q. He and L. L. Shaw, *Nanoscale*, 2015, **8**, 74–103.
16 V. S. Pradeep, M. Graczyk-Zajac, R. Riedel and G. D. Soraru, *Electrochim. Acta*, 2014, **119**, 78–85.
17 H. Fukui, Y. Harimoto, M. Akasaka and K. Eguchi, *ACS Appl. Mater. Interfaces*, 2014, **6**, 12827–12836.
18 H. Sun and K. Zhao, *ACS Appl. Mater. Interfaces*, 2017, **9**, 35001–35009.
19 P. A. Loughney, S. B. Mujib, T. L. Pruyn, G. Singh, K. Lu and V. Doan-Nguyen, *J. Appl. Phys.*, 2022, **132**, 070901.
20 P. Colombo, G. Mera, R. Riedel and G. D. Sorarù, *J. Am. Ceram. Soc.*, 2010, **93**, 1805–1837.
21 R. Bhandavat, Z. Pei and G. Singh, *Nanomater. Energy*, 2012, **1**, 324–337.
22 S. B. Mujib and G. Singh, *Int. J. Ceram. Eng. Sci.*, 2022, **4**, 4–9.
23 N. Liao, M. Zhang, B. Zheng and W. Xue, *Appl. Mater. Today*, 2020, **18**, 100434.
24 P. Dibandjo, M. Graczyk-Zajac, R. Riedel, V. S. Pradeep and G. D. Soraru, *J. Eur. Ceram. Soc.*, 2012, **32**, 2495–2503.
25 V. S. Pradeep, D. G. Ayana, M. Graczyk-Zajac, G. D. Soraru and R. Riedel, *Electrochim. Acta*, 2015, **157**, 41–45.
26 W. Z. Monika, P. Puczkarski, Z. Grabowska, J. Kaspar, M. Graczyk-Zajac, R. Riedel and G. D. Sorarù, *RSC Adv.*, 2016, **6**, 104597–104607.
27 J. Kaspar, M. Graczyk-Zajac and R. Riedel, *Solid State Ionics*, 2012, **225**, 527–531.
28 M. Halim, C. Hudaya, A.-Y. Kim and J. K. Lee, *J. Mater. Chem. A*, 2016, **4**, 2651–2656.
29 M. Weinberger, P.-H. Su, H. Peterlik, M. Lindén and M. Wohlfahrt-Mehrens, *Nanomater*, 2019, **9**, 754.
30 J. Kaspar, M. Graczyk-Zajac, S. Choudhury and R. Riedel, *Electrochim. Acta*, 2016, **216**, 196–202.
31 A. Maheshwari, E. P. Gopikrishnan, J. Gangadhar and R. Sujith, *Mater. Chem. Phys.*, 2020, **239**, 121963.
32 R. Bhandavat, M. Cologna and G. Singh, *Nanomater. Energy*, 2012, **1**, 57–61.
33 L. David, R. Bhandavat, U. Barrera and G. Singh, *Nat. Commun.*, 2016, **7**, 10998.
34 J. Shen and R. Raj, *J. Power Sources*, 2011, **196**, 5945–5950.
35 X. Lin, Y. Dong, X. Liu, X. Chen, A. Li and H. Song, *Chem. Eng. J.*, 2022, **428**, 132125.
36 E. Ionescu, H.-J. Kleebe and R. Riedel, *Chem. Soc. Rev.*, 2012, **41**, 5032–5052.
37 W. Duan, X. Yin, Q. Li, L. Schlier, P. Greil and N. Travitzky, *J. Eur. Ceram. Soc.*, 2016, **36**, 3681–3689.
38 Q. Wen, Z. Yu and R. Riedel, *Prog. Mater. Sci.*, 2020, **109**, 100623.
39 G. Barroso, Q. Li, R. K. Bordia and G. Motz, *J. Mater. Chem. A*, 2019, **7**, 1936–1963.
40 M. Arango-Ospina, F. Xie, I. Gonzalo-Juan, R. Riedel, E. Ionescu and A. R. Boccaccini, *Appl. Mater. Today*, 2020, **18**, 100482.
41 E. Bernardo, L. Fiocco, G. Parcianello, E. Storti and P. Colombo, *Mater*, 2014, **7**, 1927–1956.
42 P. Miele†, S. Bernard, D. Cornu and B. Toury, *Soft Mater.*, 2007, **4**, 249–286.
43 K. Lu, *Mater. Sci. Eng., R*, 2015, **97**, 23–49.
44 S. Fu, M. Zhu and Y. Zhu, *J. Adv. Ceram.*, 2019, **8**, 457–478.
45 M. Schulz, *Adv. Appl. Ceram.*, 2009, **108**, 454–460.
46 R. Sujith, S. Jothi, A. Zimmermann, F. Aldinger and R. Kumar, *Int. Mater. Rev.*, 2021, **66**, 426–449.
47 Q. Wen, F. Qu, Z. Yu, M. Graczyk-Zajac, X. Xiong and R. Riedel, *J. Adv. Ceram.*, 2022, **11**, 197–246.

48 A. Viard, D. Fonblanc, D. Lopez-Ferber, M. Schmidt, A. Lale, C. Durif, M. Balestrat, F. Rossignol, M. Weinmann, R. Riedel and S. Bernard, *Adv. Eng. Mater.*, 2018, **20**, 1800360.
49 W. Verbeek*Germany Pat*., DE 2218960A1, 1972.
50 S. Yajima, J. Hayashi and M. Omori, *Chem. Lett.*, 1975, **4**, 931–934.
51 G. Fritz and B. Raabe, *Z. Anorg. Allg. Chem.*, 1956, **286**, 149–167.
52 K. Bawane, D. Erb and K. Lu, *J. Eur. Ceram. Soc.*, 2019, **39**, 2846–2854.
53 C. Stabler, A. Reitz, P. Stein, B. Albert, R. Riedel and E. Ionescu, *Mater*, 2018, **11**, 279.
54 L. Wang and K. Lu, *J. Mater. Sci.*, 2019, **54**, 6073–6087.
55 R. Sujith, P. K. Chauhan, J. Gangadhar and A. Maheshwari, *Sci. Rep.*, 2018, **8**, 17633.
56 M. Wilamowska, V. S. Pradeep, M. Graczyk-Zajac, R. Riedel and G. D. Sorarù, *Solid State Ionics*, 2014, **260**, 94–100.
57 H. Fukui, H. Ohsuka, T. Hino and K. Kanamura, *J. Electrochem. Soc.*, 2013, **160**, A1276.
58 H. Lim, H. Kim, S.-O. Kim, K. J. Kim and W. Choi, *Chem. Eng. J.*, 2021, **404**, 126581.
59 G. Liu, J. Kaspar, L. M. Reinold, M. Graczyk-Zajac and R. Riedel, *Electrochim. Acta*, 2013, **106**, 101–108.
60 K. J. Lee, W. Bak, J.-J. Kim, M. A. Snyder, W. C. Yoo and Y.-E. Sung, *J. Phys. Chem. C*, 2015, **119**, 7604–7613.
61 H. Shi, A. Yuan and J. Xu, *J. Power Sources*, 2017, **364**, 288–298.
62 B. V. Manoj Kumar and Y.-W. Kim, *Sci. Technol. Adv. Mater.*, 2010, **11**, 044303.
63 M. Ma, H. Wang, M. Niu, L. Su, X. Fan, J. Deng, Y. Zhang and X. Du, *RSC Adv.*, 2016, **6**, 43316–43321.
64 K. Xia, Z. Wu, C. Xuan, W. Xiao, J. Wang and D. Wang, *Electrochim. Acta*, 2017, **245**, 287–295.
65 X. Liu, M.-C. Zheng and K. Xie, *J. Power Sources*, 2011, **196**, 10667–10672.
66 J. S. Xue, K. Myrtle and J. R. Dahn, *J. Electrochem. Soc.*, 1995, **142**, 2927.
67 H. Fukui, H. Ohsuka, T. Hino and K. Kanamura, *ACS Appl. Mater. Interfaces*, 2010, **2**, 998–1008.
68 H. Fukui, H. Ohsuka, T. Hino and K. Kanamura, *J. Electrochem. Soc.*, 2011, **158**, A550.
69 H. Fukui, K. Eguchi, H. Ohsuka, T. Hino and K. Kanamura, *J. Power Sources*, 2013, **243**, 152–158.
70 H. Fukui, H. Ohsuka, T. Hino and K. Kanamura, *J. Power Sources*, 2011, **196**, 371–378.
71 N. Liao, B. Zheng, M. Zhang and W. Xue, *J. Mater. Chem. A*, 2016, **4**, 12328–12333.
72 C. Chandra, W. Devina, H. S. Cahyadi, S. K. Kwak and J. Kim, *Chem. Eng. J.*, 2022, **428**, 131072.
73 N. Liao, B. Zheng, H. Zhou and W. Xue, *J. Mater. Chem. A*, 2015, **3**, 5067–5071.
74 N. Liao, B. Zheng, H. Zhou and W. Xue, *Electrochim. Acta*, 2015, **156**, 115–120.
75 N. Liao, B. Zheng, H. Zhou and W. Xue, *J. Power Sources*, 2016, **334**, 39–43.
76 P. Kroll, *Mater. Res. Soc. Symp. Proc.*, 2011, **1313**, 7.
77 N. Liao, M. Zhang, B. Zheng and W. Xue, *J. Phys. Chem. C*, 2019, **123**, 19315–19321.
78 M. Graczyk-Zajac, L. Reinold, J. Kaspar, P. Sasikumar, G.-D. Soraru and R. Riedel, *Nanomater*, 2015, **5**, 233–245.
79 A. P. Nowak, B. Wicikowska and A. Lisowska-Oleksiak, *Solid State Ionics*, 2014, **263**, 131–139.
80 Y. Feng, S. Dou, Y. Wei, Y. Zhang, X. Song, X. Li and V. S. Battaglia, *ACS Omega*, 2017, **2**, 8075–8085.
81 L. David, S. Bernard, C. Gervais, P. Miele and G. Singh, *J. Phys. Chem. C*, 2015, **119**, 2783–2791.
82 P. E. Sanchez-Jimenez and R. Raj, *J. Am. Ceram. Soc.*, 2010, **93**, 1127–1135.
83 S. H. Lee, C. Park, K. Do and H. Ahn, *Energy Storage Mater.*, 2021, **35**, 130–141.
84 M. Graczyk-Zajac, D. Vrankovic, P. Waleska, C. Hess, P. V. Sasikumar, S. Lauterbach, H.-J. Kleebe and G. D. Sorarù, *J. Mater. Chem. A*, 2018, **6**, 93–103.
85 D. Ahn and R. Raj, *J. Power Sources*, 2011, **196**, 2179–2186.
86 S. Nedunchezhian, R. Sujith and R. Kumar, *J. Adv. Ceram.*, 2013, **2**, 318–324.
87 R. Sujith, A. B. Kousaalya and R. Kumar, *Ceram. Int.*, 2012, **38**, 1227–1233.
88 J. Kaspar, M. Graczyk-Zajac and R. Riedel, *Solid State Ionics*, 2012, **225**, 527–531.
89 R. A. Mantz, P. F. Jones, K. P. Chaffee, J. D. Lichtenhan, J. W. Gilman, I. M. K. Ismail and M. J. Burmeister, *Chem. Mater.*, 1996, **8**, 1250–1259.
90 J. Kaspar, M. Graczyk-Zajac and R. Riedel, *J. Power Sources*, 2013, **244**, 450–455.
91 V. S. Pradeep, M. Graczyk-Zajac, M. Wilamowska, R. Riedel and G. D. Soraru, *Solid State Ionics*, 2014, **262**, 22–24.
92 V. S. Pradeep, E. Zera, M. Graczyk-Zajac, R. Riedel and G. D. Soraru, *J. Am. Ceram. Soc.*, 2016, **99**, 2977–2983.
93 P. Wu, X. Guo, Z. Su, C. Liu, S. Chen, Z. Zheng and A. Liu, *Chem. Eng. J.*, 2022, **446**, 137354.
94 M. Weinberger, C. Pfeifer, S. Schindler, T. Diemant, R. J. Behm and M. Wohlfahrt-Mehrens, *J. Mater. Chem. A*, 2015, **3**, 23707–23715.
95 H. Shi, Z. Xie, Y. Zhang, A. Yuan and J. Xu, *Ionics*, 2019, **25**, 3051–3058.
96 K. Xia, X. Liu, H. Liu, Y. Lu, Z. Liu, Y. Li, L. Duan, Z. Hou, R. Li and D. Wang, *Electrochim. Acta*, 2021, **372**, 137899.
97 S. B. Mujib, F. Ribot, C. Gervais and G. Singh, *RSC Adv.*, 2021, **11**, 35440–35454.
98 M. S. Tahir, M. Weinberger, P. Balasubramanian, T. Diemant, R. J. Behm, M. Lindén and M. Wohlfahrt-Mehrens, *J. Mater. Chem. A*, 2017, **5**, 10190–10199.
99 S. B. Mujib, R. Cuccato, S. Mukherjee, G. Franchin, P. Colombo and G. Singh, *Ceram. Int.*, 2020, **46**, 3565–3573.
100 Y. Xia, S. Cai, C. Lu, H. Huang, Y. Gan, J. Zhang, C. Liang, Z. Xiao and W. Zhang, *J. Alloys Compd.*, 2020, **816**, 152595.
101 J. Jang, H. Kim, H. Lim, K. jae Kim, H.-G. Jung, S.-O. Kim and W. Choi, *Chem. Eng. J.*, 2020, **401**, 126091.
102 J. Gangadhar, A. Maheshwari, R. K. Bordia, C. N. Shyam Kumar, C. Kubel and R. Sujith, *Ceram. Interfaces*, 2020, **46**, 28156–28164.

103 Z. Wu, X. Cheng, D. Tian, T. Gao, W. He and C. Yang, *Chem. Eng. J.*, 2019, **375**, 121997.
104 D. Knozowski, M. Graczyk-Zajac, G. Trykowski and M. Wilamowska-Zawłocka, *Mater*, 2020, **13**, 4302.
105 D. Knozowski, M. Graczyk-Zając, D. Vrankovic, G. Trykowski, M. Sawczak, D. M. De Carolis and M. Wilamowska-Zawłocka, *Composites, Part B*, 2021, **225**, 109302.
106 I. Saleh and R. Raj, *J. Power Sources*, 2016, **310**, 18–25.
107 J. Shen, D. Ahn and R. Raj, *J. Power Sources*, 2011, **196**, 2875–2878.
108 R. Bhandavat and G. Singh, *J. Phys. Chem. C*, 2013, **117**, 11899–11905.
109 H. Li, X. Yan, Z. Ma, Y. Zhang, C. Li, W. Xiao and Y. Jiang, *Ceram. Int.*, 2021, **47**, 6867–6874.
110 Y. Li, Y. Hu, Y. Lu, S. Zhang, G. Xu, K. Fu, S. Li, C. Chen, L. Zhou, X. Xia and X. Zhang, *J. Power Sources*, 2014, **254**, 33–38.
111 M. Ma, H. Wang, X. Li, K. Peng, L. Xiong and X. Du, *J. Eur. Ceram. Soc.*, 2020, **40**, 5238–5246.
112 L. David, K. M. Shareef, M. A. Abass and G. Singh, *RSC Adv.*, 2016, **6**, 53894–53902.
113 M. S. Kolathodi, L. David, M. A. Abass and G. Singh, *RSC Adv.*, 2016, **6**, 74323–74331.
114 M. Ma, H. Wang, L. Xiong, S. Huang, X. Li and X. Du, *Carbon*, 2022, **186**, 273–281.
115 Y. Ren, B. Yang, X. Huang, F. Chu, J. Qiu and J. Ding, *Solid State Ionics*, 2015, **278**, 198–202.
116 F. Ji, Y.-L. Li, J.-M. Feng, D. Su, Y.-Y. Wen, Y. Feng and F. Hou, *J. Mater. Chem.*, 2009, **19**, 9063.
117 Z. Sang, X. Yan, L. Wen, D. Su, Z. Zhao, Y. Liu, H. Ji, J. Liang and S. X. Dou, *Energy Storage Mater.*, 2020, **25**, 876–884.
118 Z. Sang, Z. Zhao, D. Su, P. Miao, F. Zhang, H. Ji and X. Yan, *J. Mater. Chem. A*, 2018, **6**, 9064–9073.
119 G. Shao, D. A. H. Hanaor, J. Wang, D. Kober, S. Li, X. Wang, X. Shen, M. F. Bekheet and A. Gurlo, *ACS Appl. Mater. Interfaces*, 2020, **12**, 46045–46056.
120 Z. Zhang, J. E. Calderon, S. Fahad, L. Ju, D.-X. Antony, Y. Yang, A. Kushima and L. Zhai, *ACS Appl. Mater. Interfaces*, 2021, **13**, 9794–9803.
121 Md. S. Islam, M. R. Karim, S. Islam, J. Kim, N. N. Rabin, R. Ohtani, M. Nakamura, M. Koinuma and S. Hayami, *ChemistrySelect*, 2016, **1**, 6429–6433.
122 L. David, R. Bhandavat, U. Barrera and G. Singh, *Nat. Commun.*, 2016, **7**, 10998.
123 H. Hong, W. Liu, M. Zhang, Y. Wang and Y. Chen, *J. Alloys Compd.*, 2021, **857**, 157476.
124 R. J. -C. Dubey, P. V. W. Sasikumar, F. Krumeich, G. Blugan, J. Kuebler, K. V. Kravchyk, T. Graule and M. V. Kovalenko, *Adv. Sci.*, 2019, **6**, 1901220.
125 D. Knozowski, P. Vallachira Warriam Sasikumar, P. Madajski, G. Blugan, M. Gazda, N. Kovalska and M. Wilamowska-Zawłocka, *Nanomaterials*, 2022, **12**, 410.
126 J. Rohrer, D. Vrankovic, D. Cupid, R. Riedel, H. J. Seifert, K. Albe and M. Graczyk-Zajac, *Int. J. Mater. Res.*, 2017, **108**, 920–932.
127 A. Tolosa, M. Widmaier, B. Krüner, J. M. Griffin and V. Presser, *Sustainable Energy Fuels*, 2017, **2**, 215–228.
128 R. J.-C. Dubey, P. V. W. Sasikumar, N. Cerboni, M. Aebli, F. Krumeich, G. Blugan, K. V. Kravchyk, T. Graule and M. V. Kovalenko, *Nanoscale*, 2020, **12**, 13540–13547.
129 D. Kim, H. Kim, H. Lim, K. J. Kim, H.-G. Jung, D. Byun, C. Kim and W. Choi, *Int. J. Energy Res.*, 2020, **44**, 11473–11486.
130 S. Dey, S. B. Mujib and G. Singh, *Nanomater.*, 2022, **12**, 553.
131 J. Kaspar, M. Graczyk-Zajac, S. Lauterbach, H.-J. Kleebe and R. Riedel, *J. Power Sources*, 2014, **269**, 164–172.
132 X. Liu, K. Xie, J. Wang, C. Zheng and Y. Pan, *J. Mater. Chem.*, 2012, **22**, 19621–19624.
133 S. Choi, D. S. Jung and J. W. Choi, *Nano Lett.*, 2014, **14**, 7120–7125.
134 D. Vrankovic, M. Graczyk-Zajac, C. Kalcher, J. Rohrer, M. Becker, C. Stabler, G. Trykowski, K. Albe and R. Riedel, *ACS Nano*, 2017, **11**, 11409–11416.
135 D. Vrankovic, K. Wissel, M. Graczyk-Zajac and R. Riedel, *Solid State Ionics*, 2017, **302**, 66–71.
136 Z. Wu, W. Lv, X. Cheng, J. Gao, Z. Qian, D. Tian, J. Li, W. He and C. Yang, *Chem.–Eur. J.*, 2019, **25**, 2604–2609.
137 W. Wei, K. Xu, N. Liao and W. Xue, *Appl. Mater. Today*, 2020, **20**, 100773.
138 J. Kaspar, C. Terzioglu, E. Ionescu, M. Graczyk-Zajac, S. Hapis, H.-J. Kleebe and R. Riedel, *Adv. Funct. Mater.*, 2014, **24**, 4097–4104.
139 C. Shi, H. Huang, Y. Xia, J. Yu, R. Fang, C. Liang, J. Zhang, Y. Gan and W. Zhang, *Chem. - Eur. J.*, 2019, **25**, 7719–7725.
140 K. Xia, L. Qu, X. Liu, H. Han, Z. Hou, Y. Li and S. Deng, *Appl. Surf. Sci.*, 2020, **506**, 144775.
141 S. E. Wang, J.-S. Park, M. Ji Kim, Y. Chan Kang and D. Soo Jung, *Appl. Surf. Sci.*, 2022, **589**, 152952.
142 M. A. Abass, A. A. Syed, C. Gervais and G. Singh, *RSC Adv.*, 2017, **7**, 21576–21584.
143 H. Huang, C. Shi, R. Fang, Y. Xia, C. Liang, Y. Gan, J. Zhang, X. Tao and W. Zhang, *Chem. Eng. J.*, 2019, **359**, 584–593.
144 G. Zhu, R. Guo, W. Luo, H. K. Liu, W. Jiang, S. X. Dou and J. Yang, *Natl. Sci. Rev.*, 2021, **8**, nwaa152.
145 J. Shen and R. Raj, *J. Power Sources*, 2011, **196**, 5945–5950.
146 B. Krüner, C. Odenwald, A. Tolosa, A. Schreiber, M. Aslan, G. Kickelbick and V. Presser, *Sustainable Energy Fuels*, 2017, **1**, 1588–1600.
147 H. T. T. Le, D. T. Ngo, X.-M. Pham, T.-Y. Nguyen, T.-D. Dang and C.-J. Park, *J. Power Sources*, 2019, **440**, 227104.
148 Q. Meng, G. Li, J. Yue, Q. Xu, Y.-X. Yin and Y.-G. Guo, *ACS Appl. Mater. Interfaces*, 2019, **11**, 32062–32068.
149 L. Jin, C. Shen, A. Shellikeri, Q. Wu, J. Zheng, P. Andrei, J.-G. Zhang and J. P. Zheng, *Energy Environ. Sci.*, 2020, **13**, 2341–2362.
150 Y. Xia, R. Fang, Z. Xiao, L. Ruan, R. Yan, H. Huang, C. Liang, Y. Gan, J. Zhang, X. Tao and W. Zhang, *RSC Adv.*, 2016, **6**, 69764–69772.
151 P. Tao, J. He, T. Shen, Y. Hao, J. Yan, Z. Huang, X. Xu, M. Li and Y. Chen, *Adv. Mater. Interfaces*, 2019, **6**, 1900460.
152 J. Wang, C. Luo, T. Gao, A. Langrock, A. C. Mignerey and C. Wang, *Small*, 2015, **11**, 473–481.

153 D. M. Soares and G. Singh, *Nanotechnol*, 2020, **31**, 145403.
154 H. Lim, S. Yu, W. Choi and S.-O. Kim, *ACS Nano*, 2021, **15**, 7409–7420.
155 Y. Lee, K. Y. Lee and W. Choi, *Adv. Funct. Mater.*, 2017, **27**, 1702607.
156 C. Chandra and J. Kim, *Chem. Eng. J.*, 2018, **338**, 126–136.
157 C. Chandra, W. Devina, S. Alvin and J. Kim, *Chem. Eng. J.*, 2021, **404**, 126520.
158 X. Dou, D. Buchholz, M. Weinberger, T. Diemant, M. Kaus, S. Indris, R. J. Behm, M. Wohlfahrt-Mehrens and S. Passerini, *Small Methods*, 2019, **3**, 1800177.
159 C. Chandra, H. S. Cahyadi, S. Alvin, W. Devina, J.-H. Park, W. Chang, K. Y. Chung, S. K. Kwak and J. Kim, *Chem. Mater.*, 2020, **32**, 410–423.
160 J. Kaspar, M. Storch, C. Schitco, R. Riedel and M. Graczyk-Zajac, *J. Electrochem. Soc.*, 2015, **163**, A156.
161 R. N. Putra, M. Halim, G. Ali, S. F. Shaikh, A. M. Al-Enizi, T. Fazal, F. J. Iftikhar and A. N. S. Saqib, *New J. Chem.*, 2020, **44**, 14035–14040.
162 H. Cheng, N. Garcia-Araez and A. L. Hector, *Mater. Adv.*, 2021, **2**, 7956–7966.
163 J. Pan, W. Zhong, Z. Gao, X. Yang, Y. Zhang, Y. Guan and X. Yan, *Ceram. Int.*, 2021, **47**, 27833–27842.
164 M. Halim, G. Liu, R. E. A. Ardhi, C. Hudaya, O. Wijaya, S.-H. Lee, A.-Y. Kim and J. K. Lee, *ACS Appl. Mater. Interfaces*, 2017, **9**, 20566–20576.
165 A. Meier, M. Weinberger, K. Pinkert, M. Oschatz, S. Paasch, L. Giebeler, H. Althues, E. Brunner, J. Eckert and S. Kaskel, *Microporous Mesoporous Mater.*, 2014, **188**, 140–148.
166 L. Duan, Q. Ma, L. Mei and Z. Chen, *Microporous Mesoporous Mater.*, 2015, **202**, 97–105.
167 A. Tolosa, B. Krüner, N. Jäckel, M. Aslan, C. Vakifahmetoglu and V. Presser, *J. Power Sources*, 2016, **313**, 178–188.
168 P. Pazhamalai, K. Krishnamoorthy, S. Sahoo, V. K. Mariappan and S.-J. Kim, *Chem. Eng. J.*, 2020, **387**, 123886.
169 U. Okoroanyanwu, A. Bhardwaj, V. Einck, A. Ribbe, W. Hu, J. M. Rodriguez, W. R. Schmidt and J. J. Watkins, *Chem. Mater.*, 2021, **33**, 678–694.
170 I. P. Swain and S. K. Behera, *Ceram. Int.*, 2022, **48**, 8216–8227.
171 M. A. Mazo, M. T. Colomer, A. Tamayo and J. Rubio, *Microporous Mesoporous Mater.*, 2022, **330**, 111604.
172 G. Jella, D. K. Panda, N. Sapkota, M. Greenough, S. P. Datta, A. M. Rao, R. Sujith and R. K. Bordia, *ACS Appl. Mater. Interfaces*, 2023, **15**, 30039–30051.

